

Reproduced by the  
**CLEARINGHOUSE**  
for Federal Scientific & Technical  
Information Springfield Va. 22151

AN INVESTIGATION OF PERFORATION  
MECHANICS IN THIN ALUMINUM PLATES

THESIS

GAW/MC/70-2

Richard D. Gabbert  
Captain            USAF

This document has been approved for public release and sale; its  
distribution is unlimited.

**AN INVESTIGATION OF PERFORATION  
MECHANICS IN THIN ALUMINUM PLATES**

**THESIS**

**Presented to the Faculty of the School of Engineering of  
the Air Force Institute of Technology  
Air University  
in Partial Fulfillment of the  
Requirements for the Degree of  
Master of Science**

**By**

**Richard D. Gabbert, B.S.A.S.E.  
Captain USAF**

**Graduate Air Weapons**

**June 1970**

**This document has been approved for public release and sale; its  
distribution is unlimited.**

Preface

This thesis represents an extension of an investigation begun by Major Thomas E. Fields, a member of AFIT class GAW-69. The velocity lost in target perforation as a function of projectile shape and target thickness was my primary area of interest.

I wish to thank Mr. Gordon H. Griffith of the Air Force Materials Laboratory for the use of range facilities; Mr. Harry Lispitt of the Aerospace Research Laboratories for advice and use of equipment; Mr. Bob Bertke, Mr. Jim Green, Mr. Charles Acton, Mr. Jack Smith, and Mr. Tom Orcutt, for their outstanding technical support and enthusiastic assistance; my faculty thesis advisor, Major William Goldberg, for his patience and guidance; and a special thanks to Mr. Jien Nishiwaki, for obvious reasons.

Richard D. Gabbert

Contents

Preface . . . . .	11
List of Figures . . . . .	v
List of Tables . . . . .	vii
Abstract . . . . .	viii
I. Introduction . . . . .	1
Background . . . . .	2
Perforation Models . . . . .	3
Purpose . . . . .	4
II. Theory . . . . .	5
Nishiwaki Theory . . . . .	5
Analysis of Nishiwaki Theory . . . . .	7
Modified Nishiwaki Theory . . . . .	7
Other Considerations . . . . .	10
Projectile Spin . . . . .	13
III. Experimental Procedure . . . . .	15
Dynamic Experiments . . . . .	15
Static Experiments . . . . .	16
IV. Results and Discussion . . . . .	18
Results of Static Experiments . . . . .	18
Discussion of Static Experiments . . . . .	23
Results of Dynamic Experiments . . . . .	26
Discussion of Dynamic Experiments . . . . .	38
V. Conclusions and Recommendations . . . . .	48
Conclusions for Static Experiments . . . . .	48
Conclusions for Dynamic Experiments . . . . .	49
Overall Conclusions . . . . .	49
Recommendations . . . . .	50
Bibliography . . . . .	51
Appendix A: Description of Equipment . . . . .	53
Gun . . . . .	53
Sabot Catch Tank . . . . .	53
Contact Switches . . . . .	55

Contents (cont'd)

Chronographs . . . . .	55
Flash X-Ray System . . . . .	55
Static Test Equipment . . . . .	56
Appendix B: Projectile Design . . . . .	58
Projectile Sabots . . . . .	58
Experimental Projectiles . . . . .	60
Appendix C: Data and Data Reduction . . . . .	62
Initial Velocity Data . . . . .	62
Impact Velocity Data . . . . .	62
X-ray Measurements . . . . .	62
Static Pressure Measurements . . . . .	63
Appendix D: Solution of Nishiwaki Equations . . . . .	65
Vita . . . . .	68

List of Figures

<u>Figure</u>		<u>Page</u>
1	Common Types of Plate Failure . . . . .	2
2	Nishiwaki Model . . . . .	5
3	Alternate Analysis of Nishiwaki Model . . . .	8
4	Free Body Diagram of Alternate Analysis of Nishiwaki Model . . . . .	9
5	Modified Nishiwaki Model . . . . .	12
6	Possible Analysis of Initial Impact . . . . .	12
7	Possible Model for Further Investigation . .	14
8	Relative Force vs. Time Curves for Cylindrical Projectile Against 0.476 cm Target at Cross Head Speeds of 0.846, 0.0846, and 0.00846 cm/sec . . . . .	19
9	Typical Curves for Ball Projectile Against Varied Target Thickness . . . . .	20
10	Typical Force vs Time Curves in Quasi-Static Tests Against 0.317 cm Targets . . . . .	21
11	Typical Force vs Time Curves in Quasi-Static Tests Against 0.317 cm Targets . . . . .	22
12	Results of Low Temperature Perforation By a Cylindrical Projectile Against Various Target Thickness . . . . .	25
13	Comparison of Velocity Loss Prediction Error for Ogive Projectiles . . . . .	40
14	Comparison of Velocity Loss Prediction Error for Optimal Projectiles . . . . .	41
15	Comparison of Velocity Loss Prediction Error for Russian Projectiles . . . . .	42
16	Comparison of Velocity Loss Prediction Error for Ball Projectiles . . . . .	43
17	Comparison of Velocity Loss Prediction Error for Cone #1 Projectiles . . . . .	44

<u>Figure</u>		<u>Page</u>
18	Comparison of Velocity Loss Prediction Error for Cone #2 Projectiles . . . . .	45
19	Predicted Ballistic Limit of 6061-T6 Aluminum Impacted by Cylindrical Projectiles . . . . .	47
20	Range Layout . . . . .	54
21	Schematic of Instron Model TT . . . . .	57
22	Experimental Sabot . . . . .	58
23	Comparison of Projectile Nose Shapes . . . . .	59



List of Tables

<u>Table</u>		<u>Page</u>
I	Results for 0.159 cm 6061-T6 Aluminum Targets	27
II	Results for 0.317 cm 6061-T6 Aluminum Targets	28
III	Results for 0.476 cm 6061-T6 Aluminum Targets	29
IV	Comparison of Theoretical Velocity Losses for Shots Against 0.159 cm 6061-T6 Aluminum Targets . . . . .	30
V	Comparison of Theoretical Velocity Losses for Shots Against 0.317 cm 6061-T6 Aluminum Targets . . . . .	31
VI	Comparison of Theoretical Velocity Losses for Shots Against 0.476 cm 6061-T6 Aluminum Targets . . . . .	32
VII	Accuracy of Theoretical Predictions of Residual Velocities for Shots Against 0.159 cm 6061-T6 Aluminum Targets . . . . .	33
VIII	Accuracy of Theoretical Predictions of Residual Velocities for Shots Against 0.317 cm 6061-T6 Aluminum Targets . . . . .	34
IX	Accuracy of Theoretical Predictions of Residual Velocities for Shots Against 0.476 cm 6061-T6 Aluminum Targets . . . . .	36

Abstract

The Nishiwaki theory of penetration was investigated for seven projectile shapes against three thicknesses of 6061-T6 aluminum target material. The projectiles were fired from a 50 caliber gun at impact velocities near 500 m/sec. Initial velocities and projectile velocity losses were measured by flash x-rays and chronographs.

The same projectile shapes were also used to perforate identical targets quasi-statically with a laboratory universal testing machine. This provided the empirical information necessary to the application of the Nishiwaki theory.

The basic Nishiwaki equations were found to be inaccurate for most projectile shapes. A modification of this theory was investigated and found to be accurate in predicting projectile velocity losses to within 8 m/sec at impact velocities near 500 m/sec. Additional proposed penetration models are presented but not investigated.

AN INVESTIGATION OF PERFORATION  
MECHANICS IN THIN ALUMINUM PLATES

I. Introduction

At the present time there is no analytic method to incorporate survivability and vulnerability engineering into the initial design of a combat aircraft. There is a large amount of empirical data collected through testing and evaluation of combat damage in Southeast Asia, but no single model has yet been developed to predict the vulnerability of a given aircraft structure against a known threat. If ballistic perforation of thin targets were predictable with sufficient accuracy, the results could be used in the design of aircraft armor.

Several theories on deformation and failure of thin plates have been advanced, attempting to create mathematical relationships among projectile mass, geometry, and impact velocity; and target density, strength, and thickness. Thus far, none of the theories advanced are entirely consistent with experimental data.

The purpose of this study is to investigate the effect of projectile shape on the perforation of thin aluminum plates. This is an extension of an investigation by Major Thomas E. Fields (Ref 6) and data collected during that study is used in this paper. Residual projectile velocity as a function of projectile geometry during normal impact and the force history during perforation are the primary areas of interest. Special attention is given to the Nishiwaki model (Ref 12).

### Background

This study is concerned with the perforation of a target by a projectile, rather than merely the penetration. In penetration, the projectile does not pass completely through the target, but merely enters it. In perforation, the projectile enters the target, passes through, and proceeds with some significant velocity (Ref 13:198). Since the study of survivability is concerned with the potential damage to be caused by a projectile after perforation of an aircraft skin, the aspect of mere penetration is ignored.

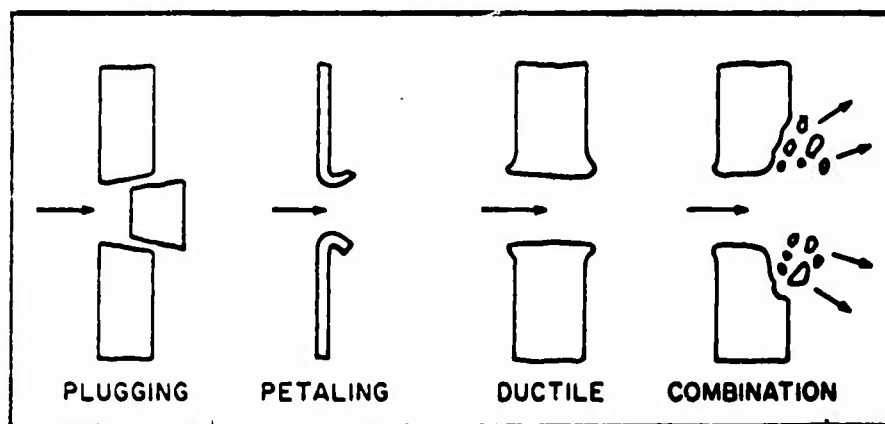


Fig. 1. Common Types of Plate Failure  
(From Ref 13:206-207)

Previous investigations indicate perforation involves crack formation, spalling, elastic and plastic wave propagation, friction and heating, and projectile shattering (Ref 9:241). Target failure is usually through plugging, petaling, ductile fracture, or a combination of the three (Ref 13:206-207). At impact velocities less than 3,000 ft/sec, thinner plates usually fail by petaling while in thicker plates plugging is most common. At higher velocities, all thicknesses of plate fail by plugging (Ref 6:2). Thus far, several simplified

models have been advanced to explain various failure modes.

#### Perforation Models

For ductile failure, Bethe (Ref 2) and Taylor (Ref 15) analyze the propagation of a circular hole in a thin plastic sheet. They consider an infinite sheet penetrated by a pointed conical projectile. The equilibrium elastic and plastic stress distributions are then analyzed. The target inertia effects were incorporated into the above work by Freiburger (Ref 7). Craggs (Ref 5) used an analogy between a thin flexible wire and a plastic membrane to attempt creation of a ductile model.

Momentum considerations have resulted in numerous theories of thin plates. Zaid and Burton (Ref 17) have derived a good approximation for high velocity projectiles. They assume inertia forces are much greater than material strength and failure will be through petaling. Nishiwaki (Ref 12) related the pressure exerted by the projectile on the target to the momentum of the displaced target material. He assumes target material is displaced normal to the projectile surface under constant static pressure and variable dynamic pressure. The variable dynamic pressure is predicted and the static pressure determined from static tests. For failure by plugging, various models have been proposed to relate velocity drop in the projectile to plug momentum and the energy needed to shear the plug from the target (Ref 8,9,14).

Thomson (Ref 14) has expanded on the Taylor hole enlargement theory, assuming a dish type perforation pattern. He considers the energy dissipated in plastic work, heat from friction, and the accel-

eration of displaced target particles.

Purpose

All the proposed theories assume either a specific nature of target failure or a definite projectile shape. The purpose of this study is to measure actual velocity losses of several projectile shapes perforating thin aluminum targets at ballistic velocities and to obtain force histories of these projectiles through the same targets at constant known strain rates of various magnitudes. These velocity losses and force histories will be compared with values calculated from the Nishiwaki model. An attempt will be made to refine the equations of the Nishiwaki model to provide more accurate correlations with experimental data.

## II. Theory

### Nishiwaki Theory (Ref 12)

Mr. Jien Nishiwaki has proposed a model in which the total resistance to motion of a penetrating projectile is a function of dynamic and static pressures. He assumes the displaced target material remains in contact with the projectile nose, resulting in his expression for dynamic pressure. He assumes a constant static pressure for a given material and thickness which can be determined by static tests. For the projectile in Fig. 2 the normal and friction forces acting on an incremental surface area  $dA$ , are:

$$F_N = P_0 \text{ and } F_f = kP_0 \quad (1)$$

where  $k$  is the static friction coefficient.

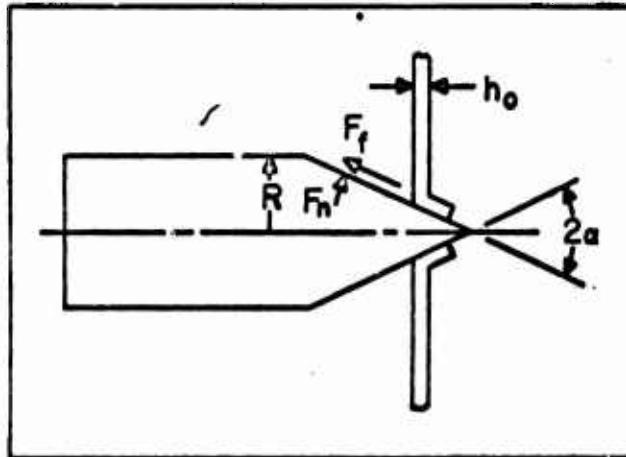


Fig. 2. Nishiwaki Model (From Ref 6:10)

For a projectile moving slowly through a target, the resistance to motion is given by:

$$dR_0 = P_0 dA (\sin \alpha + k \cos \alpha) \quad (2)$$

Assuming the particles of target material contacted are pushed back normal to the projectile surface, their velocity would be equal to the

component of projectile velocity normal to the projectile surface.

The momentum of the material displaced per unit time may be expressed:

$$(\rho V dA) \sin \alpha \cdot V \sin \alpha \quad (3)$$

where  $\rho$  is the target density and  $V$  is the velocity of the projectile.

Therefore, the dynamic pressure is given by:

$$\rho V^2 \sin^2 \alpha \quad (4)$$

The total resistance to projectile motion would be the sum of the static and dynamic forces acting on the projectile surface.

$$dR = (P_0 + \rho V^2 \sin^2 \alpha) dA (\sin \alpha + k \cos \alpha) \quad (5)$$

Assuming the frictional forces are of sufficiently small magnitude to be ignored, the equation of motion for a projectile of mass  $M$  is:

$$M \frac{dV}{dt} = - \int_A (P_0 + \rho V^2 \sin^2 \alpha) \sin \alpha dA \quad (6)$$

Assuming a projectile of conical shape, no projectile deformation, and a target thickness less than  $R/\tan \alpha$ , Eq (6) may be solved for the residual projectile velocity,  $V_r$ , where:

$$V_r^2 = - \frac{P_0}{\rho \sin^2 \alpha} + \left( V^2 + \frac{P_0}{\rho \sin^2 \alpha} \right) e^{- \frac{2\pi \rho R^2 h_0 \sin^2 \alpha}{M}} \quad (7)$$

Nishiwaki performed several tests to determine the static pressure for aluminum plates of various thicknesses. As a result of the tests, he found the static pressure to be a linear function of thickness as in the equation:

$$P_0 = 5.4 h_0 \quad (8)$$

where  $P_0$  is in  $\text{kg/mm}^2$ , and  $h_0$  is measured in mm.

The Nishiwaki model does not consider the energy dissipated in elastic and plastic wave propagation, target crack formation, projec-



tile deformation, projectile instability after impact, or possible changes in static pressure as a function of impact velocity and other factors.

#### Analysis of Nishiwaki Theory

A closer look at the Nishiwaki Model presents at least one dilemma. No provision is made to provide an unoccupied volume into which the displaced target particles may be propelled. Another analysis, consistent with all Nishiwaki assumptions may be considered. Instead of considering the particles in immediate contact on the target/projectile interface to be displaced normal to the projectile surface, one may assume that target particles are displaced from the face opposite impact, normal to the surface of the projectile with a velocity equal to the component of projectile velocity in that direction.

Target particles remaining in the projectile path could be considered to be in static equilibrium until dislodged from the back face. An example of this analysis is shown in Fig. 3. The resulting free body diagram of this analysis is shown in Fig. 4. The equations of motion for the diagram in Fig. 4 produce the same resultant equation of motion for the system as derived by Nishiwaki. This derivation is included in Appendix D.

#### Modified Nishiwaki Theory

Results obtained by Fields (Ref 6) and data collected during this study indicate a large percent of error in predicting projectile residual velocities with the Nishiwaki equations. In addition, experimental evidence indicates the formation of plugs by virtually all shapes given a target of sufficient thickness. The plugs are not necessarily

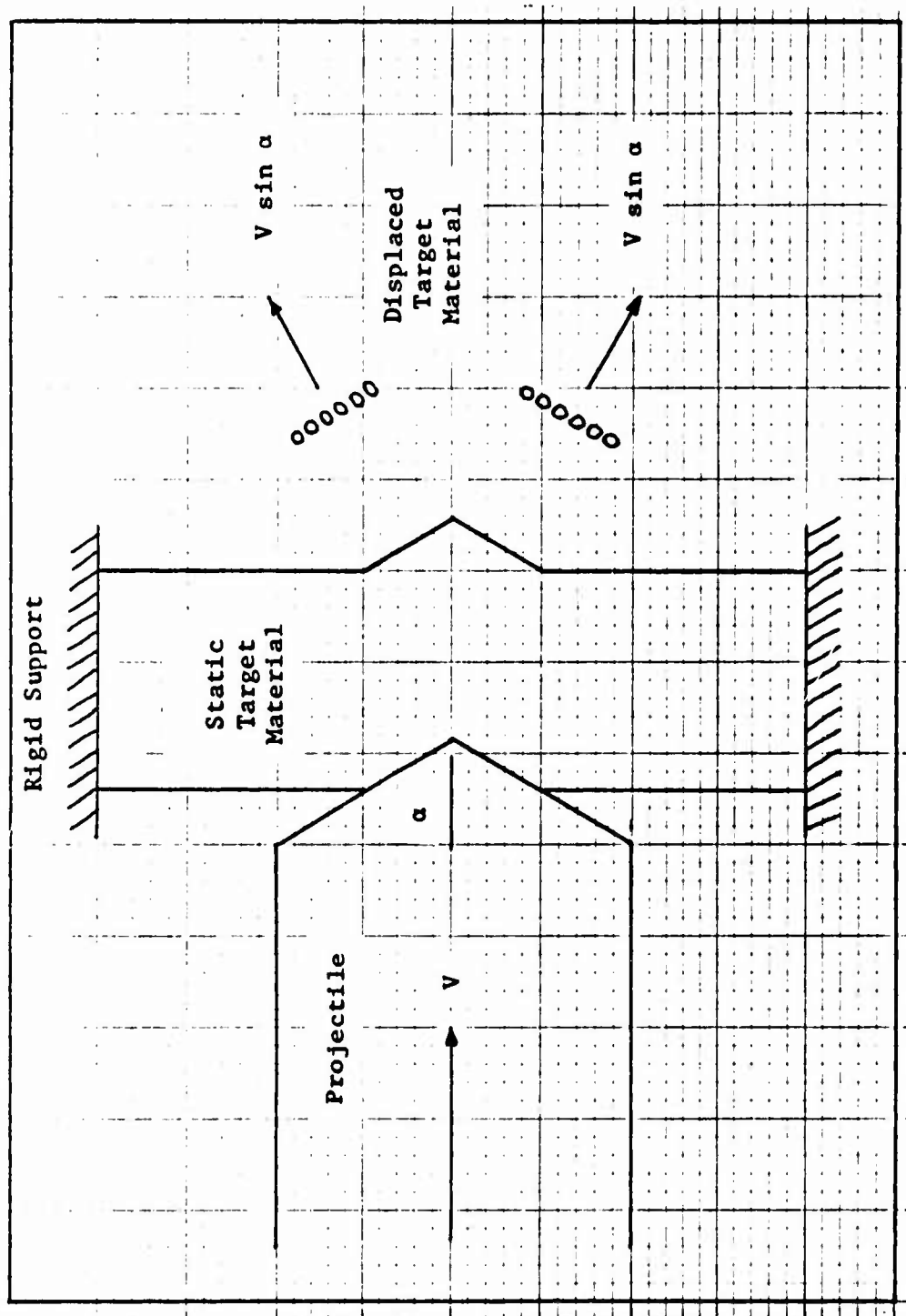


Fig. 3. Alternate Analysis of Nishiwaki Model

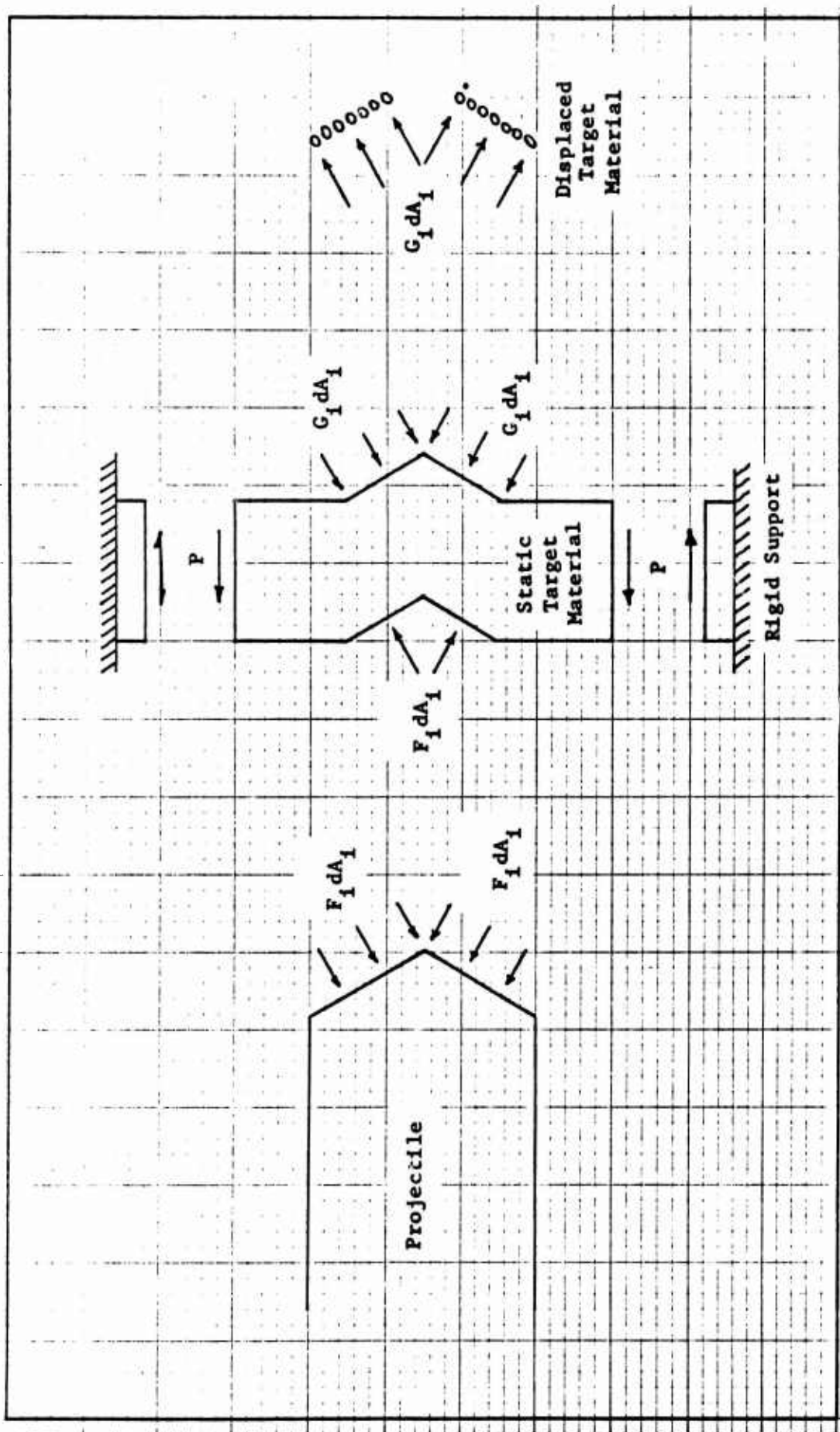


Fig. 4. Free Body Diagram of Alternate Analysis of Nishiwaki Model

the diameter of the projectiles. Plugs were observed both in the dynamic experiments of Fields (Ref 6) and in the static and dynamic tests performed in this study. As a result, a Modified Nishiwaki Theory is proposed. Consider the same set of assumptions proposed by Nishiwaki with one exception; instead of displacing the target particles normal to the projectile surface with a velocity equal to the component of projectile velocity in that direction, let the particles be displaced in a direction along the projectile trajectory with a velocity equal to that of the projectile. The resulting differential equation for the system in this analysis would be:

$$M \frac{dV}{dt} = \int_A (P_0 + \rho V^2) dA \quad (9)$$

While the original Nishiwaki analysis is somewhat unrealistic in that, with the exception of the cylinder, no projectile will produce a plug, the modified analysis is also in error since it implies a plug equal in diameter to the projectile for all projectiles. For purposes of this study, the Nishiwaki and Modified Nishiwaki analyses will be studied and their relative accuracy in predicting velocity loss compared.

#### Other Considerations

As will be shown later in this report, the basic Nishiwaki equations tend to predict less of a velocity drop than is observed in testing. The mathematical results of the Nishiwaki equations are the virtual elimination of shape effects in penetration while minimizing the magnitude of the dynamic effects in discharging a plug (Appendix D). The mathematical results of the Modified Nishiwaki equations are

also the elimination of shape effects while apparently exaggerating the dynamic effects in discharging a plug, if any. To account for shape effects and other impact phenomena, several other approaches to the same basic analysis are offered. One analysis might consider the Nishiwaki model of penetration with all the appropriate assumptions up to some arbitrary depth of penetration. At this point, the material remaining in the target in the path of the projectile could be discharged in the direction of the projectile trajectory with a velocity equal to that of the projectile. The proposed diameter of the plug formed could be determined experimentally. A proposed model of this analysis is given in Fig. 5.

In addition to the generation of plugs, many projectiles have a cratering effect on the impacted face of the target. A "ring" of target material is often observed surrounding the perforation on the impacted face. A model to account for this behavior and the variable size plugging phenomena could be considered. Assume during the initial stages of impact target particles are ejected from the impacted face of the target, tangent to the projectile face, with a horizontal component of velocity equal in magnitude and opposite in direction to the velocity of the projectile (Fig. 6). At some arbitrary point to be determined experimentally, the particles would no longer be ejected from the impacted surface of the target, but would be discharged from the back surface, normal to the projectile surface with a velocity equal to the component of projectile velocity in that direction. Then, at a second point to be determined experimentally, a plug is formed which is ejected along the trajectory with projectile velocity, while the remaining material is continuously displaced as

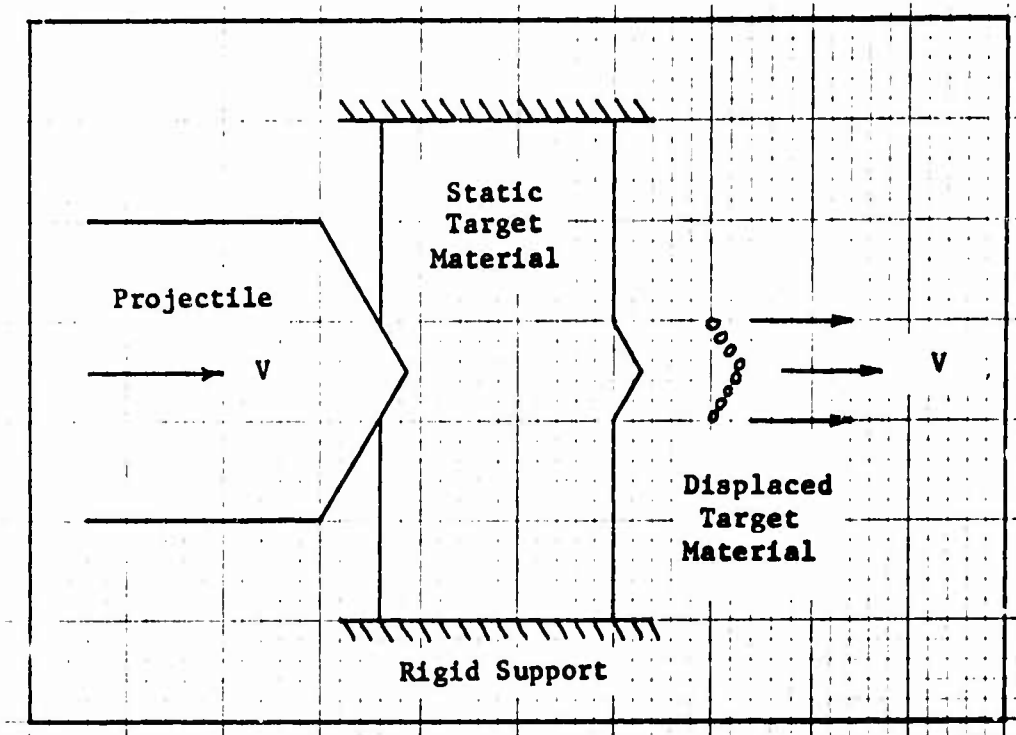


Fig. 5. Modified Nishiwaki Model

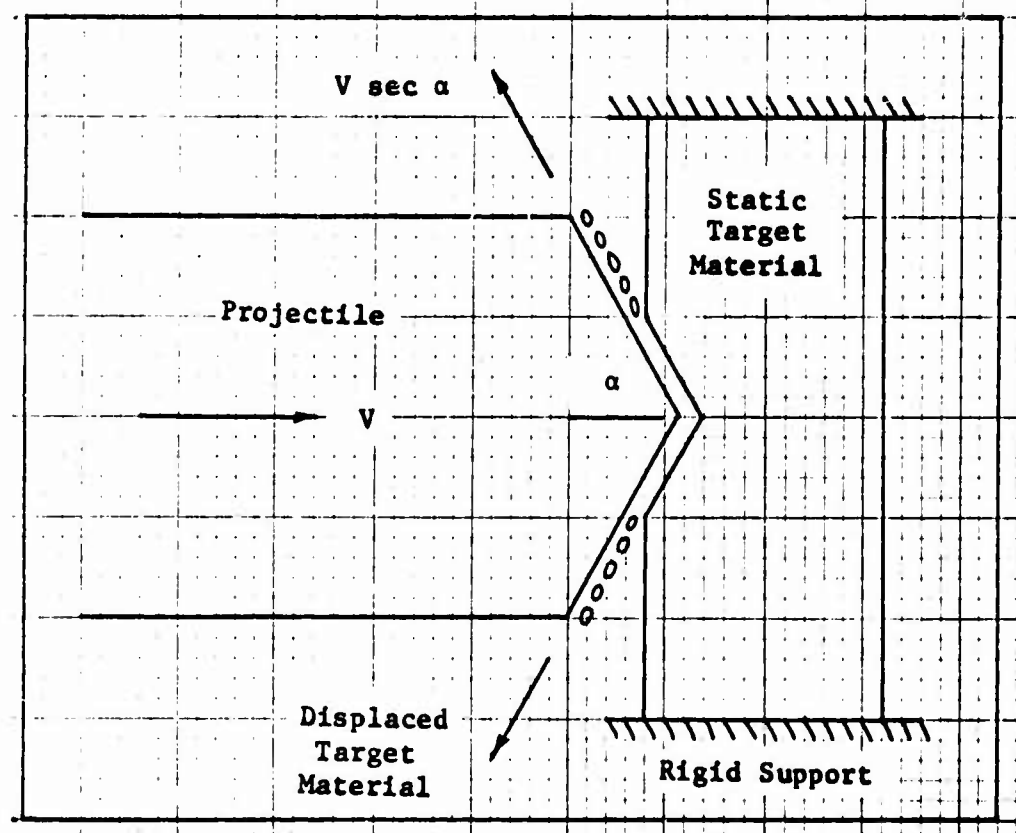


Fig. 6. Possible Analysis of Initial Impact

stated above. This proposed model would account for target material on the impact face, different plug sizes for various projectile shapes, and spallation around the exit hole of the target. An example of this analysis is shown in Fig. 7.

#### Projectile Spin

Velocity losses due to projectile spin and sliding friction were considered negligible in this study. Results of both experimental and theoretical analyses by Thomson (Ref 16) and Krafft (Ref 10) indicate losses of this nature vary from 3% to less than 1% of the energy of the projectile prior to impact.

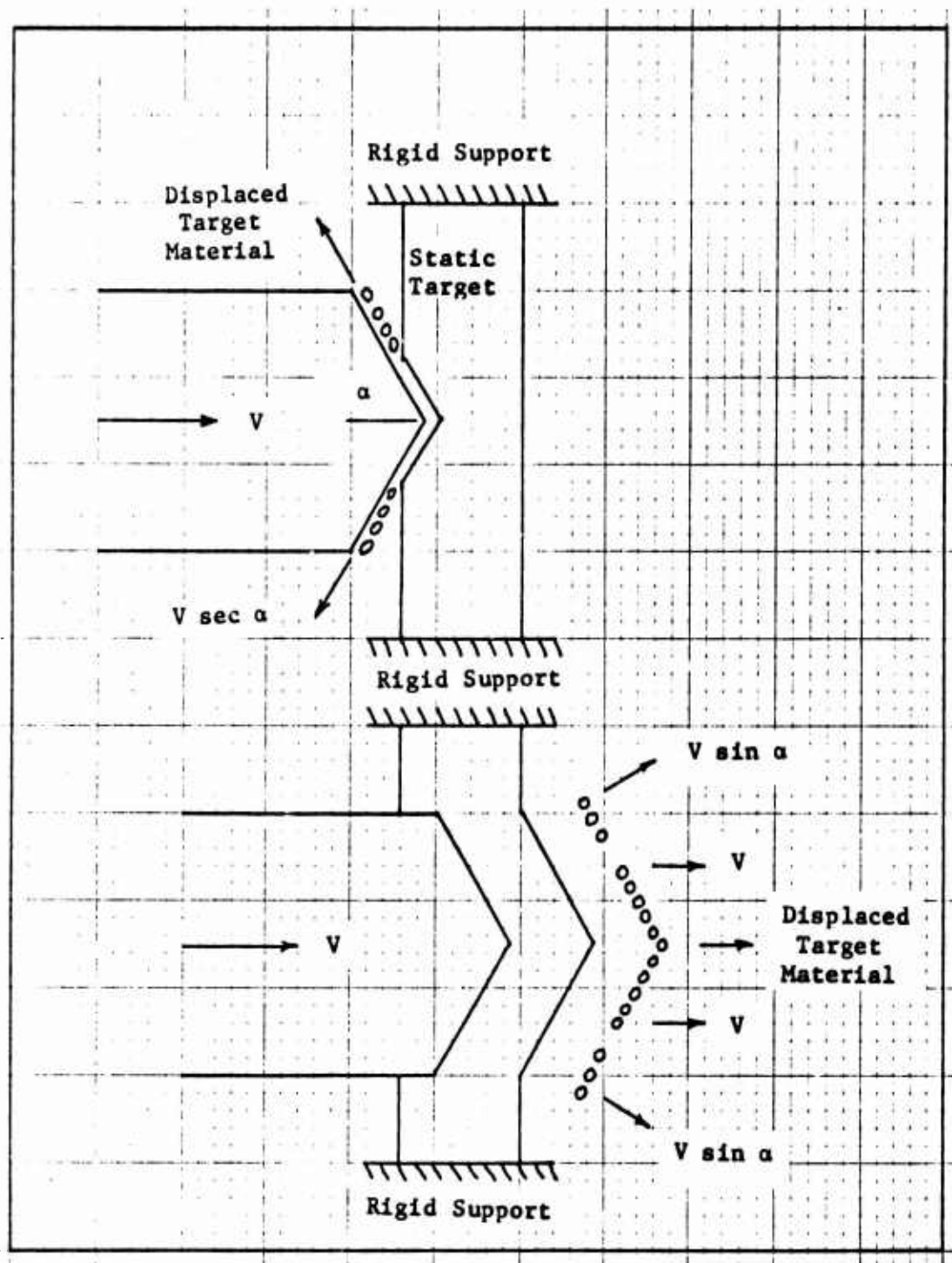


Fig. 7. Possible Model for Further Investigation



### III. Experimental Procedure

The six projectile shapes used in this analysis were the "Ogive," "Russian," "Optimal," "Cone," "Cylinder," and "Ball." The Ogive shape is identical to the core of a standard U.S. 50 caliber armor piercing bullet. The Russian shape was designed after the core of a Russian 14.5mm armor piercing bullet (Ref 4). The Optimal shape was patterned from Kucher's equation of an optimal penetrator for thin plates (Ref 11). The Cylinder is merely a flat-ended right circular cylinder. Two Cone shapes were used in the study and will be referred to as Cone #1 and Cone #2. Cone #1 is a right circular cone with a 45 degree semi-vertex angle and Cone #2 is a similar cone with a 15.1 degree semi-vertex angle. The Ball shape nose was rounded into a hemisphere with radius equal to that of the projectile body. The diameter of all projectiles was  $1.11 \pm 0.01$  cm. A complete description of the projectiles is given in Appendix B. Both static and dynamic experiments were performed with all projectile shapes on various thicknesses of 6061-T6 aluminum.

#### Dynamic Experiments

A description of the procedure used in dynamic testing of the Ogive, Russian, Cylinder, Cone #1, and Optimal projectile shapes is included in Reference 6. The resultant data from that investigation has been extracted and is used in this study.

The average mass of the Ball projectiles was 20.82 gm with a maximum deviation of 0.21 gm. The average mass of the Cone #2 projectiles was 22.38 gm with a maximum deviation of 0.22 gm. The differences in mass in different projectile shapes are due to stability requirements.

To obtain a desired impact velocity of 520 m/sec, a load of 80 grains of Dupont IMR 4064 powder was used for Ball shape and a load of 85 grains for Cone #2. Cloth cleaning patches were used to fill the remainder of the cartridge. Projectiles were seated by crimping the cartridge neck into the sabot crimping ring. The average impact velocity of the ball shape was 519.73 m/sec with a maximum deviation of 18.72 m/sec. For the Cone #2 shape, the average impact velocity was 535.02 m/sec with a maximum deviation of 9.07 m/sec. The difference in velocities within each shape is due to gas leakage around the sabots and variations in projectile masses. A description of equipment used and firing range geometry is included in Appendix A. Initial velocity contact switches provided the time required for the projectile to traverse a given distance. A camera triggered by a witness plate provided evidence of projectile stability and proper orientation immediately prior to impact. Residual projectile velocities were obtained from flash X-ray photographs triggered by contact switches after impact. These photos also confirmed proper projectile stability, lack of deformation, and orientation after impact.

#### Static Experiments

To study the static pressure component of resistance in the Nishiwaki model, various thicknesses of 6061-T6 aluminum were penetrated at various rates by all six projectile shapes. Plots of force applied versus time were obtained during the penetration process. During the quasi-static penetration tests, the targets were constrained in such a manner as to confine the area of deformation to that experienced in dynamic testing. Three penetration rates were employed, all differing

by a factor of ten. The three rates were 8.46, 0.846, and 0.046 mm/sec. These tests were performed on the prototype Instron Model TT, which is described in Appendix A. This machine records the total force applied as a function of cross head displacement while applying a load at a constant velocity. It is felt these penetration rates closely simulate static conditions.

#### IV. Results and Discussion

##### Results of Static Experiments

The relative consistency of results for the quasi-static experiments is shown in Fig. 8. This figure contains the results for the penetration of a plate of 0.476 cm 6061-T6 aluminum at crosshead speeds of 8.46, 0.846, and 0.0846 mm/sec, by a cylindrical projectile 1.11 cm in diameter. The peak forces recorded during penetration at these velocities were 6100, 6180, and 6110 pounds, respectively. The maximum deviation from the arithmetic mean, in this case, was less than one percent. The Nishiwaki static pressure coefficient ( $P_0$ ) was determined from the results obtained from the penetration of cylindrical projectiles. The average experimental values of  $P_0$  were found to be:

7.17 kg/mm<sup>2</sup> for 0.159 cm targets

17.8 kg/mm<sup>2</sup> for 0.317 cm targets

28.7 kg/mm<sup>2</sup> for 0.476 cm targets

The typical change in the nature of force versus time curves obtained for different thicknesses of targets for the ball projectile is shown in Fig. 9. The average peak forces recorded during this experiment were found to be 1317, 2773, and 5107 pounds for targets of 0.159, 0.317, and 0.476 cm thickness.

The typical nature of the force versus time curves obtained for all shapes against 0.317 cm targets is displayed in Figs. 10 and 11. The average peak forces recorded during these tests are as follows:

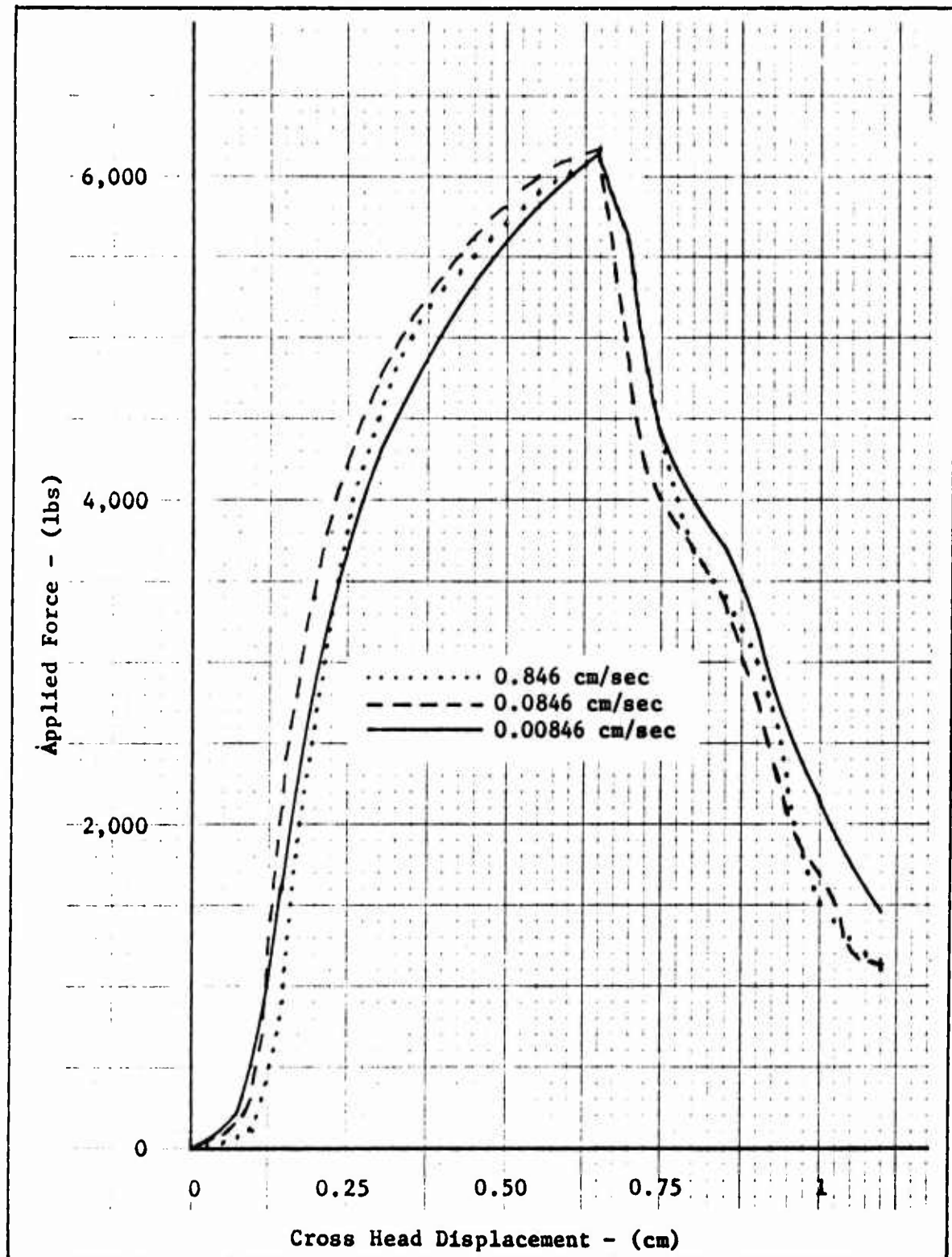


Fig. 8. Relative Force vs. Time Curves for Cylindrical Projectile Against 0.476 cm Target at Cross Head Speeds of 0.846, 0.0846, and 0.00846 cm/sec

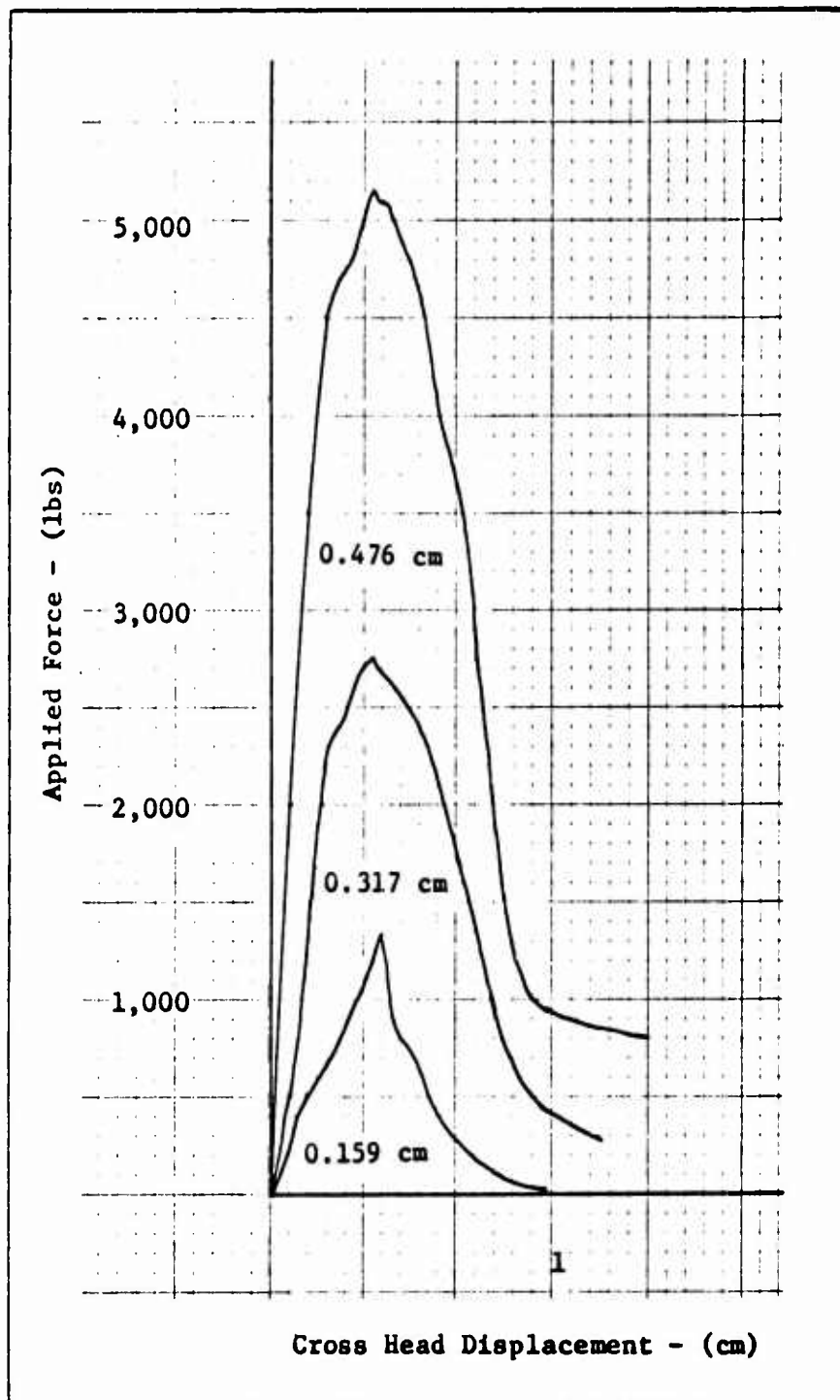


Fig. 9. Typical Curves for Ball Projectile Against Varied Target Thickness

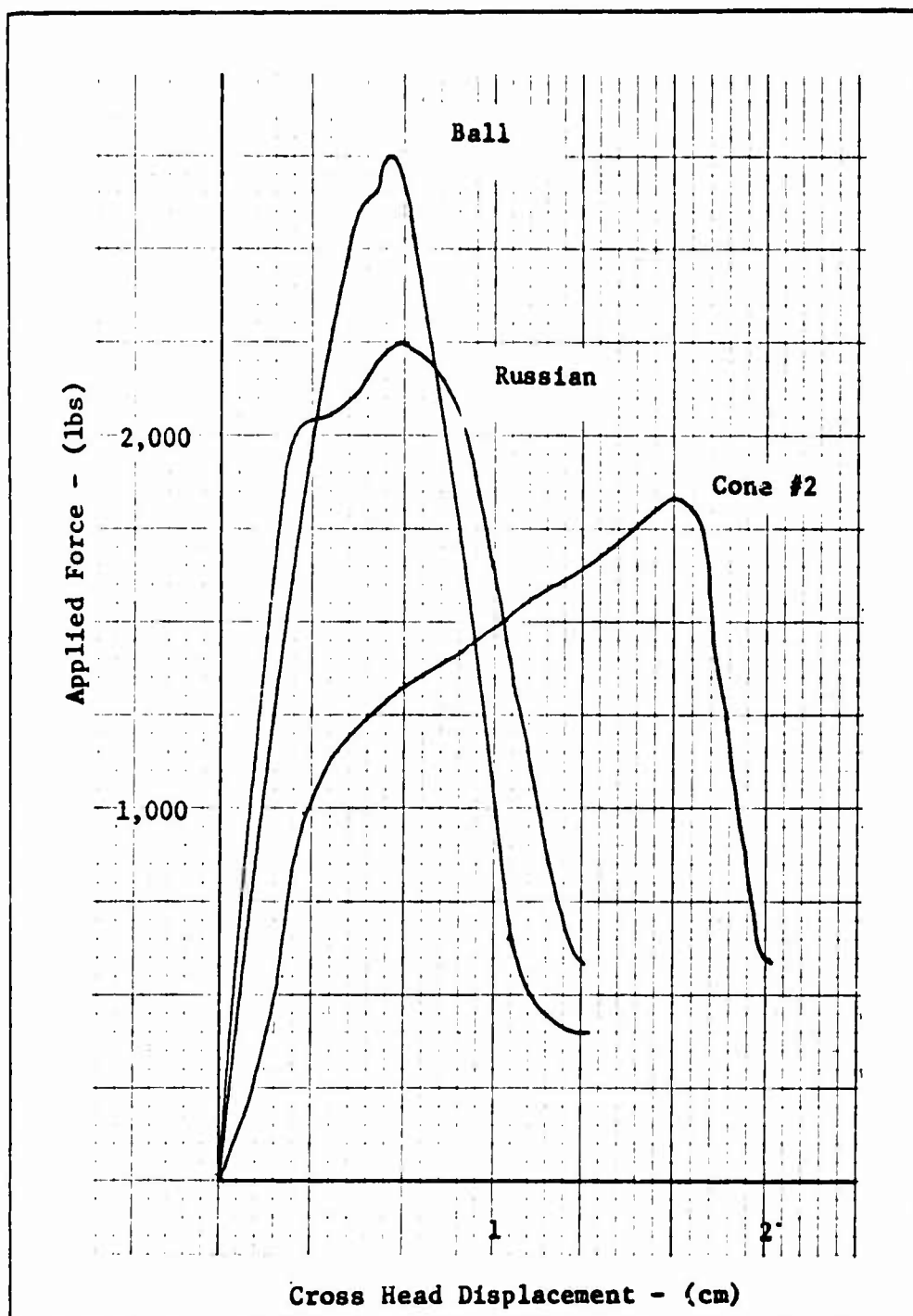


Fig. 10. Typical Force vs. Time Curves in Quasi-Static Tests Against 0.317 cm Targets

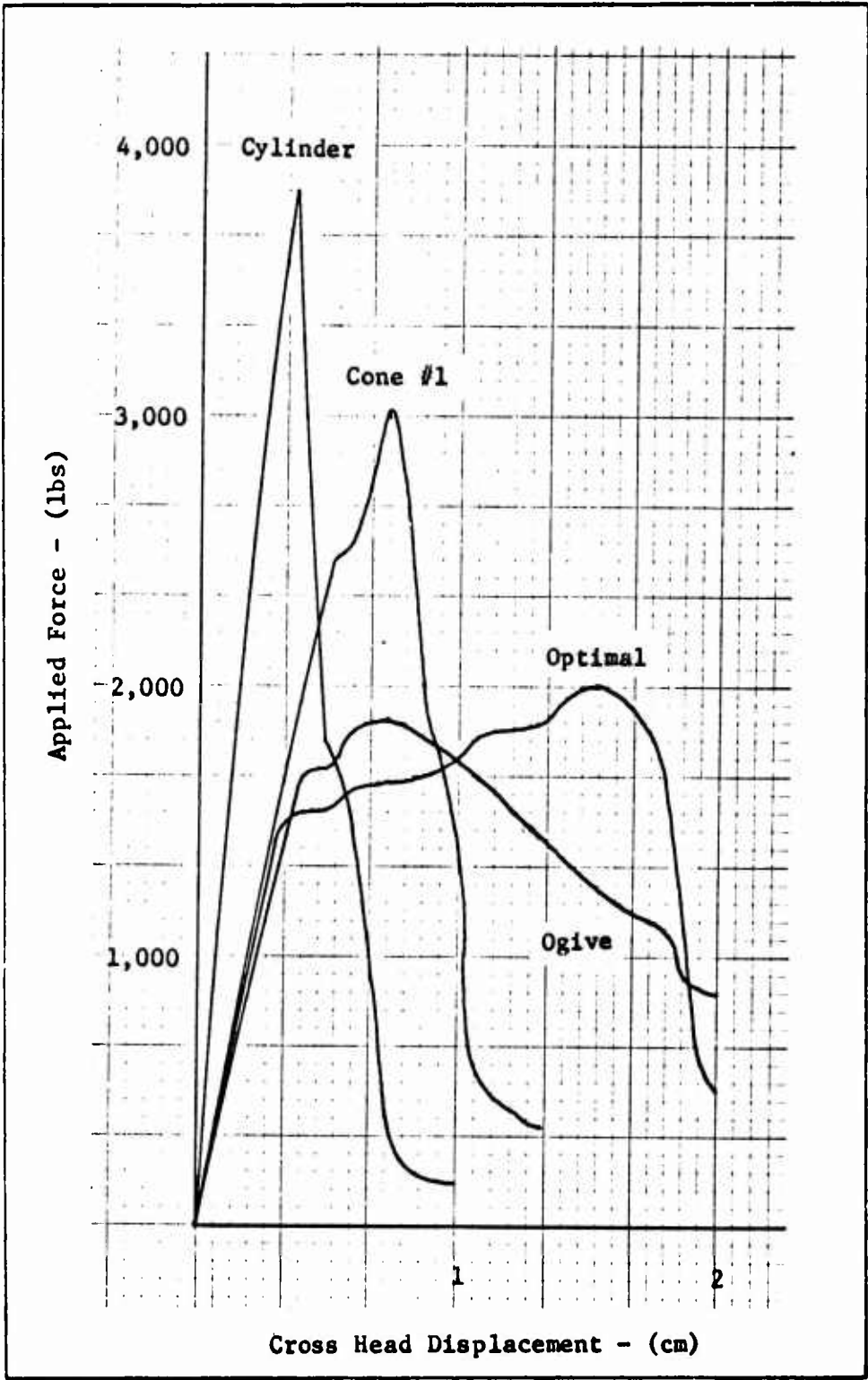


Fig. 11. Typical Force vs. Time Curves in Quasi-Static Tests Against 0.317 cm Targets



Cylinder	3,813 pounds
Cone #1	3,003 pounds
Ball	2,773 pounds
Russian	2,250 pounds
Cone #2	2,000 pounds
Ogive	1,930 pounds
Optimal	1,830 pounds

It is interesting to note that the peak force observed during penetration by the various projectile shapes is consistent with the relative efficiency of the projectiles as stated by Fields (Ref 6).

#### Discussion of Static Experiments

To determine the static pressure coefficient ( $P_0$ ), Nishiwaki applied a constant pressure to an aluminum plate and let the rate of penetration vary. The lowest value of pressure that resulted in the complete perforation of the target was used by Nishiwaki as the value of  $P_0$ . In this study, a varying pressure was applied to the target at a constant velocity and the peak value of pressure recorded during perforation by a cylindrical projectile was used as the value of  $P_0$ . The cylinder was the only projectile to offer a known area of contact between the target and projectile up to the point of fracture of the target material. The average peak value of pressure was used because it was necessary to achieve that value to result in perforation. Values of  $P_0$  obtained in this manner closely approximate those determined by Nishiwaki. Attempts were made to confirm the value of  $P_0$  from other projectile shapes but the results were inconclusive. The area of interface between projectile and target were calculated from

the Nishiwaki model and a commonly accepted value of a friction coefficient between dissimilar metals of 0.5 was used to calculate the maximum recorded load expected during quasi-static tests on various shapes. The result of this analysis, both including and excluding friction, indicated a much lower value of  $P_0$  for various curved shapes than was determined for the cylinder. It is felt, however, that these tests were not conclusive since the actual area of interface could not accurately be determined and although the target after static impact closely resembled one after dynamic impact, it could not be assumed that the static tests on curved shapes closely approximated a dynamic impact. Therefore, for purposes of this study, the values of  $P_0$  determined from tests with cylindrical projectiles were used and assumed universal for the given thicknesses of target material.

Since Butcher and Karnes (Ref 3) found that certain material properties were a function of strain rate, an additional test to find this dependence was performed. Target plates of all three thicknesses were perforated in quasi-static tests performed at  $-193^{\circ}\text{C}$  by pouring liquid nitrogen over the targets during the entire perforation process. It was hoped that this technique would be a static simulation of a high velocity perforation. The resulting curves obtained were similar in behavior for all projectile shapes when compared with results obtained at room temperature (see Fig. 12). The percentage change in peak force was different for each shape at a given target thickness and the relative change for each shape at different thicknesses was not consistent with the behavior at room temperature. The implications of these results are that  $P_0$  is not a linear function of target thickness for any shape at low or high impact velocities,

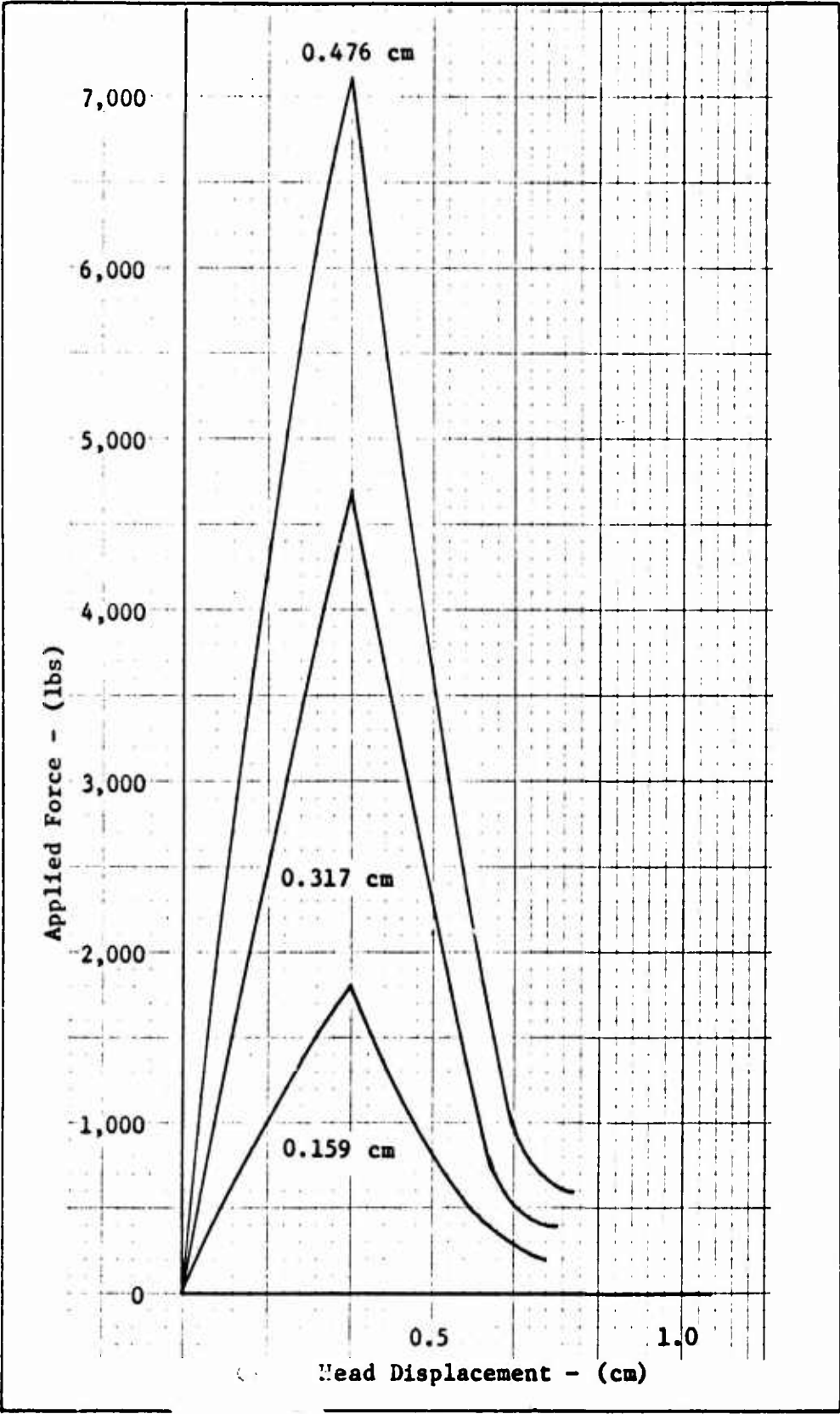


Fig. 12. Results of Low Temperature Perforation  
By a Cylindrical Projectile Against Various  
Target Thickness

$P_0$  is not a constant value for all shape projectiles, and  $P_0$  is a function of impact velocity. It was not determined what impact velocity was simulated in the low temperature tests, but the results for the cylinder indicated an increase in  $P_0$  of 17% for 0.159 cm targets, 23% for 0.317 cm targets, and 16% for 0.476 cm targets. Although there is evidence to the contrary, for purposes of this analysis the experimentally determined values of  $P_0$  were assumed to be universal for a given thickness and constant over the impact velocity range used.

An examination of the perforated targets showed no visible difference between those used in static experiments and those perforated in dynamic experiments. In addition, a similar behavior in plugging was noted in both types of experiments.

#### Results of Dynamic Experiments

Table I through III list the experimental results for the seven projectile shapes for each target thickness. The tables include projectile mass, impact velocity, perforation velocity loss, ratio of velocity loss to impact velocity, and the ratio of kinetic energy loss to impact energy. Tables IV through VI list a comparison of actual experimental projectile velocity losses with those predicted by Nishiwaki and those resulting from the Modified Nishiwaki analysis. The quasi-static values of  $P_0$ , as found on page 18, were used in all calculations. Tables VII through IX compare the error between actual projectile velocity losses and those predicted by the two forms of the Nishiwaki analysis. Error is expressed in both difference in velocity loss and percent of velocity loss. Positive error is defined to be an over-prediction. That is, the predicted velocity loss is

Table I  
Results for 0.159 cm 6061-T6 Aluminum Targets

Shape	Shot No.	Mass (gm)	Impact Velocity $V_0$ (m/sec)	Perforation Velocity Loss $\Delta V$ (m/sec)	$\frac{\Delta V}{V_0}$	$\frac{\Delta E}{E_0}$
Ogive	2F	19.34*	535.59*	7.22*	0.0135*	0.0268*
Ogive	3	19.25*	529.74*	6.98*	0.0132*	0.0262*
Optimal	4	19.35*	517.70*	7.19*	0.0139*	0.0276*
Optimal	5	19.37*	518.77*	7.16*	0.0138*	0.0274*
Russian	7F	19.73*	507.98*	12.34*	0.0234*	0.0480*
Russian	57	19.75*	499.35*	12.53	0.0251*	0.0495*
Cone #1	9F	19.70*	507.19*	14.69*	0.0290*	0.0571*
Cone #1	10F	19.71*	515.45*	14.81*	0.0287*	0.0566*
Cylinder	58	19.89*	476.01*	13.75*	0.0289*	0.0569*
Cylinder	59	19.88*	508.98*	11.46*	0.0225*	0.0445*
Ball	2	20.77	523.68	12.41	0.0237	0.0468
Ball	15	21.03	525.96	11.61	0.0221	0.0437
Cone #2	9	22.60	544.09	5.66	0.0104	0.0207

\*Indicates data obtained by Fields (Ref 6)

Table II  
Results for 0.317 cm 6061-T6 Aluminum Targets

Shape	Shot No.	Mass (gm)	Impact Velocity $V_0$ (m/sec)	Perforation Velocity Loss $\Delta V$ (m/sec)	$\frac{\Delta V}{V_0}$	$\frac{\Delta E}{E_0}$
Ogive	13F	19.39*	485.73*	23.07*	0.0475*	0.0927*
Ogive	14F	19.32*	489.45*	24.14*	0.0493*	0.0962*
Ogive	56	19.28*	555.89*	20.57*	0.0370*	0.0726*
Optimal	12F	19.31*	518.56*	22.77*	0.0438*	0.0859*
Optimal	15F	19.59*	521.30*	24.72*	0.0474*	0.0926*
Optimal	16	19.24*	528.25*	24.66*	0.0467*	0.0912*
Optimal	41	18.59*	497.37*	24.35*	0.0490*	0.0955*
Russian	23	19.82*	528.37*	24.69*	0.0466*	0.0909*
Russian	25	19.80*	497.95*	26.43*	0.0531*	0.1033*
Cone #1	22	19.78*	531.39*	32.49*	0.0611*	0.1185*
Cone #1	24	19.82*	505.97*	30.05*	0.0594*	0.1152*
Cylinder	26	19.87*	480.97*	26.61*	0.0553*	0.1076*
Cylinder	27	19.89*	480.82*	27.92*	0.0581*	0.1128*
Ball	1	20.68	501.01	31.98	0.0638	0.1236
Ball	14	20.94	525.03	29.30	0.0558	0.1085
Cone #2	8	22.36	526.92	28.82	0.0547	0.1064
Cone #2	12	22.16	541.94	24.94	0.0460	0.0899

\*Indicates data obtained by Fields (Ref 6)

Table III  
Results for 0.476 cm 6061-T6 Aluminum Targets

Shape	Shot No.	Mass (gm)	Impact Velocity V <sub>o</sub> (m/sec)	Perforation Velocity Loss ΔV (m/sec)	$\frac{\Delta V}{V_o}$	$\frac{\Delta E}{E_o}$
Ogive	28	19.32*	529.74*	36.06*	0.0681*	0.1315*
Ogive	29	19.28*	520.17*	38.31*	0.0736*	0.1419*
Optimal	39	18.29*	488.99*	41.18*	0.0842*	0.1613*
Optimal	40	18.82*	526.15*	35.84*	0.0681*	0.1316*
Russian	31	19.79*	503.99*	41.27*	0.0819*	0.1571*
Russian	42	19.24*	496.21*	42.49*	0.0856*	0.1639*
Cone #1	32	19.79*	512.68*	52.21*	0.1018*	0.1933*
Cone #1	33	19.69*	520.32*	48.16*	0.0926*	0.1765*
Cone #1	43	19.92*	472.10*	50.32*	0.1066*	0.2018*
Cone #1	55	19.76*	514.81*	51.51*	0.1011*	0.1901*
Cylinder	34	19.87*	497.55*	44.84*	0.0901*	0.1721*
Cylinder	36	19.88*	489.23*	44.84*	0.0916*	0.1749*
Ball	10	20.64	525.47	44.05	0.0838	0.1606
Ball	13	20.86	517.22	45.42	0.0878	0.1679
Cone #2	7	22.39	527.14	32.85	0.0623	0.1208

\*Indicates data obtained by Fields (Ref 6)

Table IV  
Comparison of Theoretical Velocity Losses for Shots Against 0.159 cm 6061-T6 Aluminum Targets

Experimental Data				Nishiwaki Theory		Modified Nishiwaki Theory	
Shape	Shot	Mass (gm)	Impact Velocity (m/sec)	Velocity Loss (m/sec)	Velocity Loss (m/sec)	Velocity Loss (m/sec)	Velocity Loss (m/sec)
Ogive	2F	19.34*	535.59*	7.22*	1.04	12.43	12.43
Ogive	3	19.25*	529.74*	6.98*	1.06	12.37	12.37
Russian	7F	19.73*	507.89*	12.34*	1.08	11.66	11.66
Russian	57	19.75	499.35	12.53*	1.10	11.49	11.49
Ball	2	20.77	523.68	12.41	1.00	11.37	11.37
Ball	15	21.03	525.96	11.61	0.98	11.26	11.26
Cone #1	9F	19.70*	507.19*	14.69*	6.40	11.67	11.67
Cone #1	10F	19.71*	515.45*	14.81*	6.47	11.82	11.82
Cylinder	58	19.89*	476.01*	13.75*	10.98	10.98	10.98
Cylinder	59	19.88	508.98*	11.46*	11.60	11.60	11.60
Cone #2	9	22.60	544.09	5.66	1.56	10.79	10.79
Optimal	5	19.37*	518.77*	7.16*	1.08	12.08	12.08

\*Indicates data obtained by Fields (Ref 6)



Table V  
Comparison of Theoretical Velocity Losses for Shots Against 0.317 cm 6061-T6 Aluminum Targets

Experimental Data			Nishiwaki Theory		Modified Nishiwaki Theory
Shape	Shot	Mass (gm)	Impact Velocity (m/sec)	Velocity Loss (m/sec)	Velocity Loss (m/sec)
Optimal	12F	19.31*	518.56*	22.77*	5.38
Optimal	15F	19.59*	521.30*	24.72*	5.28
Optimal	16	19.24*	528.25*	24.66*	5.30
Optimal	19	19.41*	519.90*	23.10	5.34
Optimal	41	18.59*	497.37*	24.35*	5.83
Ogive	13F	19.39*	485.73*	23.07*	5.73
Ogive	14F	19.32*	489.45*	24.14*	5.70
Ogive	56	19.28*	555.89*	20.57*	5.02
Russian	23	19.82*	528.37*	24.60*	5.14
Russian	25	19.80	497.95*	26.43	5.47
Ball	1	20.68	501.01	31.98	5.20
Ball	14	20.94	525.03	29.30	4.90
Cone #1	22	19.78	531.39	32.49	16.13
Cone #1	24	19.82*	505.97*	30.05*	15.83
Cylinder	26	19.87*	480.97*	26.61*	25.28
Cylinder	27	19.89*	480.82*	27.92*	25.25
Cone #2	8	22.36	526.92	28.82	5.89
Cone #2	12	22.16	541.94	24.94	5.85

\*Indicates data obtained by Fields (Ref 6)

Table VI  
Comparison of Theoretical Velocity Losses for Shots Against 0.476 cm 6061-T6 Aluminum Targets

Experimental Data				Nishivaki Theory		Modified Nishivaki Theory
Shape	Shot	Mass (gm)	Impact Velocity (m/sec)	Velocity Loss (m/sec)	Velocity Loss (m/sec)	Velocity Loss (m/sec)
Ogive	28	19.32	529.74*	36.06*	12.80	45.85
Ogive	29	19.28	520.17*	38.31*	13.07	45.58
Optimal	39	18.29*	488.99*	41.18*	14.69	46.86
Optimal	40	18.82*	526.15*	35.84*	13.24	46.90
Russian	31	19.79*	503.99*	41.27*	13.15	43.86
Russian	42	19.24*	496.21*	42.49	13.75	44.83
Ball	10	20.64	525.47	44.05	12.07	42.82
Ball	13	20.86	517.22	45.42	12.14	42.09
Cone #1	32	19.79*	512.58*	52.21*	28.78	44.16
Cone #1	33	19.69*	520.32*	48.16*	28.97	44.66
Cone #1	43	19.92*	472.10*	50.32*	28.48	42.56
Cone #1	55	19.76*	514.81*	51.51*	28.83	44.31
Cylinder	34	19.87*	497.55*	44.84*	43.48	43.48
Cylinder	36	19.88*	489.23*	44.84*	43.18	43.18
Cone #2	7	22.39	527.14	32.85	13.07	39.58

\*Indicates data obtained by Fields (Ref 6)

Table VII  
Accuracy of Theoretical Predictions of Residual Velocities for Shots Against 0.159 cm 6061-T6 Aluminum Targets

Shape	Shot No.	Nishiwaki Theory				Modified Nishiwaki			
		$\Delta V_A$ m/sec	$\Delta V_P$ m/sec	Error m/sec	Error %	$\Delta V_P$ m/sec	Error m/sec	Error %	
Ogive	2F	7.22*	1.04	-6.18	-85.6	12.43	5.21	72.2	
Ogive	3	6.98*	1.06	-5.92	-84.8	12.37	5.39	77.2	
Optimal	5	7.16*	1.08	-6.08	-84.9	12.08	4.92	68.7	
Russian	7F	12.34*	1.08	-11.26	-91.2	11.66	-0.68	-5.5	
Russian	57	12.53*	1.10	-11.43	-91.2	11.49	-1.04	-8.3	
Cone #1	9F	14.69*	6.40	-8.29	-56.4	11.67	-3.02	-20.6	
Cone #1	10F	14.81*	6.47	-8.34	-56.3	11.82	-2.99	-20.2	
Cylinder	58	13.75*	10.98	-2.77	-20.1	10.98	-2.77	-20.1	
Cylinder	59	11.46*	11.60	0.14	1.2	11.60	-2.77	-20.1	
Ball	2	12.41	1.00	-11.41	-91.9	11.37	-1.04	-8.4	
Cone #2	9	5.66	1.56	-4.10	-72.4	10.79	5.13	90.8	

$\Delta V_A$  = actual projectile velocity loss

$\Delta V_P$  = predicted projectile velocity loss

Error (m/sec) =  $\Delta V_P - \Delta V_A$

Error (%) =  $(\Delta V_P - \Delta V_A) \times 100 / \Delta V_A$

\*Indicates data obtained by Fields (Ref 6)

Table VIII  
Accuracy of Theoretical Predictions of Residual Velocities for Shots Against 0.317 cm 6061-T6 Aluminum Targets

Shape	Shot No.	Nishiwaki Theory				Modified Nishiwaki			
		$\Delta V_A$ m/sec	$\Delta V_P$ m/sec	Error m/sec	Error %	$\Delta V_P$ m/sec	Error m/sec	Error %	Error %
Ogive	13F	23.07*	5.73	-17.34	-75.1	26.04	2.97	12.9	12.9
Ogive	14F	24.14*	5.70	-18.44	-76.5	26.24	2.10	8.7	8.7
Ogive	56	20.57*	5.02	-15.55	-75.8	28.40	7.83	38.1	38.1
Optimal	12F	22.77*	5.38	-17.39	-76.4	27.16	4.39	19.3	19.3
Optimal	15F	24.72*	5.28	-19.44	-78.8	26.86	2.14	8.7	8.7
Optimal	16	24.66*	5.30	-19.36	-78.5	27.56	2.90	11.7	11.7
Optimal	19	23.10*	5.34	-17.76	-76.9	27.06	3.96	17.1	17.1
Optimal	41	24.35*	5.83	-18.52	-76.3	27.49	3.14	12.9	12.9
Russian	23	24.60*	5.14	-19.46	-79.1	26.77	2.17	8.8	8.8
Russian	25	26.43*	5.47	-20.96	-76.1	25.87	-0.56	2.1	2.1
Ball	1	31.98	5.20	-26.78	-83.8	24.88	-7.10	-22.2	-22.2
Ball	14	29.30	4.90	-24.40	-83.3	25.26	-4.04	-13.8	-13.8

$\Delta V_A$  = actual projectile velocity loss

$\Delta V_P$  = predicted projectile velocity loss

Error (m/sec) =  $\Delta V_P - \Delta V_A$

Error (%) =  $(\Delta V_P - \Delta V_A) \times 100 / \Delta V_A$

\*Indicates data obtained by Fields (Ref 6)

Table VIII (cont'd)  
Accuracy of Theoretical Predictions of Residual Velocities for Shots Against 0.317 cm 6061-T6 Aluminum Targets

Shape	Shot No.	Nishiwaki Theory				Modified Nishiwaki			
		$\Delta V_A$ m/sec	$\Delta V_P$ m/sec	Error m/sec	Error %	$\Delta V_P$ m/sec	Error m/sec	Error %	
Cone #1	22	32.49*	16.13	-16.36	-50.4	26.92	-5.57	-17.1	
Cone #1	24	30.05*	15.83	-14.22	-47.4	26.09	-3.96	-13.2	
Cylinder	26	26.61	25.28	-1.33	-5.0	25.28	-1.33	-5.0	
Cylinder	27	27.92*	25.25	-1.67	-5.9	25.25	-1.67	-5.9	
Cone #2	8	28.82	5.89	-22.93	-79.4	23.73	-5.09	-17.6	
Cone #2	12	24.94	5.85	-19.09	-76.6	24.36	-0.58	-2.3	

$\Delta V_A$  = actual projectile velocity loss

$\Delta V_P$  = predicted projectile velocity loss

Error (m/sec) =  $\Delta V_P - \Delta V_A$

Error (%) =  $(\Delta V_P - \Delta V_A) \times 100 / \Delta V_A$

\*Indicates data obtained by Fields (Ref 6)

Table IX  
of Theoretical Predictions of Residual Velocities for Shots Against 0.476 cm 6061-T6 Aluminum Targets

Shape	Shot No.	Nishiwaki Theory				Modified Nishiwaki			
		AVA m/sec	AVP m/sec	Error m/sec	Error %	AVP m/sec	Error m/sec	Error %	
Ogive	28	36.06*	12.80	-23.26	-66.3	45.85	9.79	27.1	
Ogive	29	38.31*	13.07	-25.24	-66.0	45.58	7.27	19.0	
Optimal	39	41.18*	14.69	-26.49	-64.3	46.86	5.66	13.8	
Optimal	40	35.84*	13.24	-22.60	-63.0	46.90	11.06	30.8	
Russian	31	41.27*	13.15	-28.12	-68.1	43.86	2.59	6.3	
Russian	42	42.49*	13.75	-28.74	-67.8	44.83	2.34	5.5	
Ball	10	44.05	12.07	-31.98	-72.5	42.82	-1.23	-2.8	
Ball	13	45.42	12.14	-33.28	-73.4	42.09	-3.33	-7.3	
Cone #1	32	52.21*	28.78	-23.43	-45.0	44.16	-8.05	-15.4	
Cone #1	33	48.16*	28.97	-19.19	-39.8	44.66	-3.50	-7.3	
Cone #1	43	50.32*	28.48	-21.84	-43.5	42.56	-7.76	-15.4	
Cone #1	55	51.51*	23.83	-22.68	-44.0	44.31	-7.20	-13.9	

AVA = actual projectile velocity loss

AVP = predicted projectile velocity loss

Error (m/sec) = AVP-AVA

Error (%) = (AVP-AVA) x 100/AVA

\*Indicates data obtained by Fields (Ref 6)

Table IX (cont'd)

Accuracy of Theoretical Predictions of Residual Velocities for Shots Against 0.476 cm 6061-T6 Aluminum Targets

Shape	Shot No.	Nishiwaki Theory				Modified Nishiwaki			
		$\Delta V_A$ m/sec	$\Delta V_P$ m/sec	Error m/sec	Error %	$\Delta V_P$ m/sec	Error m/sec	Error %	Error %
Cylinder	34	44.84*	43.48	-1.36	-3.0	43.48	-1.36	-3.0	
Cylinder	36	44.84*	43.18	-1.66	-3.7	43.18	-1.66	-3.7	
Cone #2	7	32.85	13.07	-19.78	-60.3	39.58	6.73	20.4	

$\Delta V_A$  = actual projectile velocity loss

$\Delta V_P$  = predicted projectile velocity loss

Error (m/sec) =  $\Delta V_P - \Delta V_A$

Error (%) =  $(\Delta V_P - \Delta V_A) \times 100 / \Delta V_A$

\*Indicates data obtained by Fields (Ref 6)

greater than that found experimentally. Negative error is defined to be an under-prediction. In this case the predicted velocity loss is less than the experimental velocity loss.

Against 0.159 cm targets, the difference between the actual residual velocity and the predicted residual velocity varied from an average of only 1.36 m/sec for the cylinder projectile to 11.34 m/sec for the Russian shape. For targets of 0.317 cm thickness, the average error varied from 2.00 m/sec for the cylinder to 25.59 m/sec for the ball shape. For 0.476 cm targets, the average error ranged from 1.51 m/sec for the cylinder to 32.65 m/sec for the ball. These errors were determined using the basic Nishiwaki equations. In all cases the velocity loss predicted by the Nishiwaki equations was less than the actual velocity loss.

The Modified Nishiwaki equations resulted in errors of a lesser magnitude. Against 0.159 cm targets, the average error ranged from only 0.86 m/sec for the Russian shape up to 5.30 m/sec for the Ogive. For targets 0.317 cm thick, the average error varied from only 0.81 m/sec for the Russian projectile up to 5.52 m/sec for the Ball. Against 0.476 cm targets, the average error ranged from 1.51 m/sec for the cylinder up to 8.38 m/sec for the Optimal.

#### Discussion of Dynamic Experiments

The reliability of the dynamic tests is determined by how closely the basic assumptions were met. It may be assumed the testing performed by Fields (Ref 6) adequately met the assumed conditions. For experiments with the ball and cone #2 shape projectiles, normal



impact orientation was confirmed through photographs of the projectile immediately prior to impact. Projectile stability and the absence of projectile deformation after impact was corroborated by X-ray pictures taken immediately after impact. For the Ball and Cone #2 projectiles, only those experiments meeting the assumptions stated above were used as data points.

The Nishiwaki assumption that target particles are displaced normal to the projectile surface was partially discredited by dynamic experiments on the Ball shape and static experiments on all shapes. X-ray photographs of the Ball projectile immediately after impact reveal a plug leading the projectile. The diameter of the plug closely approximated that of the projectile, implying dynamic effects similar to that of the Cylinder shape projectile. Static testing revealed similar behavior for this projectile. In addition, it was discussed that all shapes of projectiles tend to create plugs, given a sufficiently thick target. In light of the above, it is not surprising that the Modified Nishiwaki Theory is more accurate in predicting residual velocities.

The magnitude of error in predicting residual velocities for the curved shapes is in agreement with the relative penetration efficiency of the projectiles as determined by Fields (Ref 6). A comparison of the average percent error in predicting velocity loss for all projectiles against all target thicknesses used is given in Figs. 13 through 18. It can be seen that the error in the Modified Nishiwaki predictions corresponds to the probable plug size. For example, the Optimal and Cone #2 projectiles, which would produce the smallest plugs, reveal the greatest error. Assuming a smaller plug size would decrease the

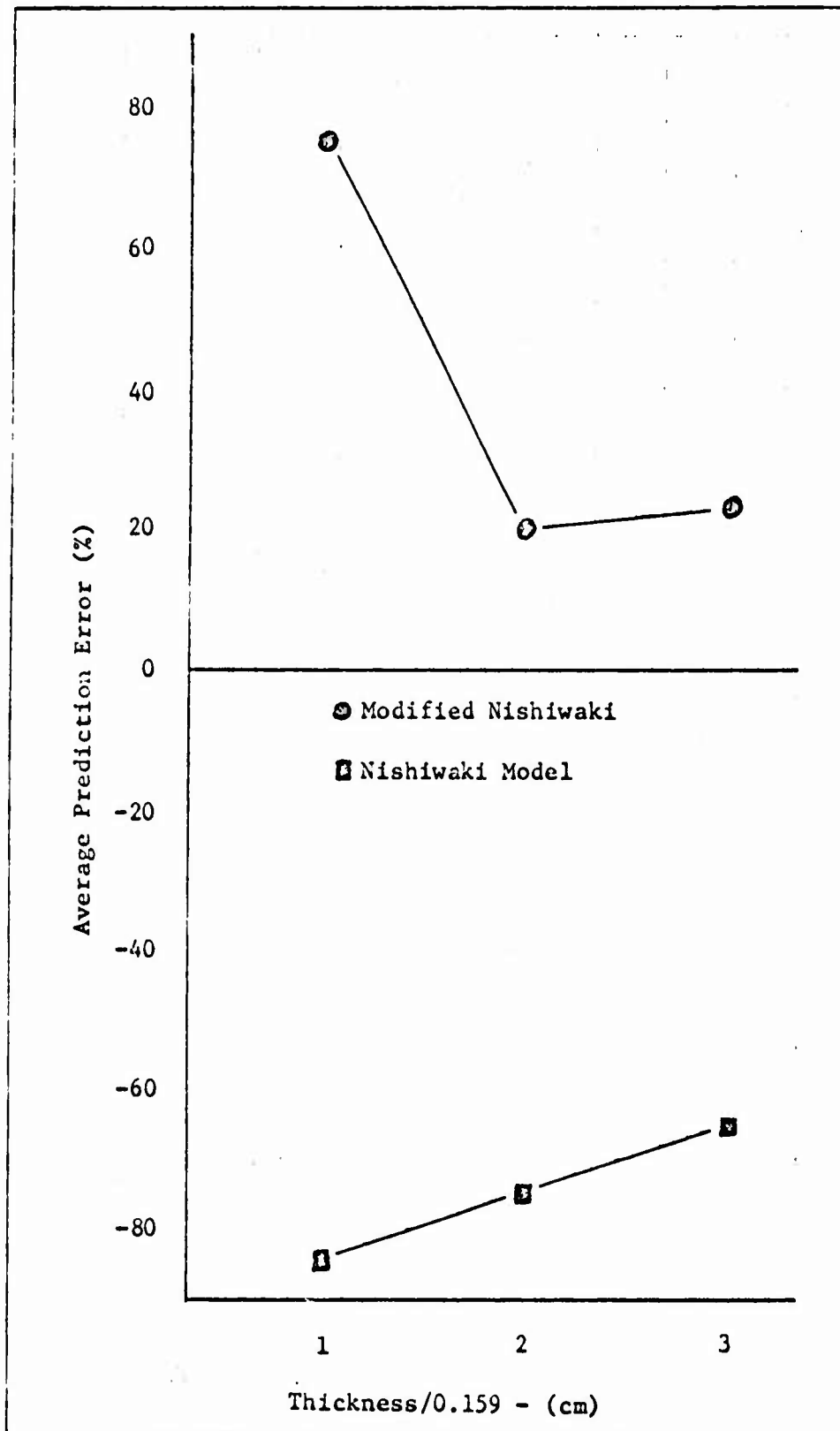


Fig. 13. Comparison of Velocity Loss Prediction Error for Ogive Projectiles

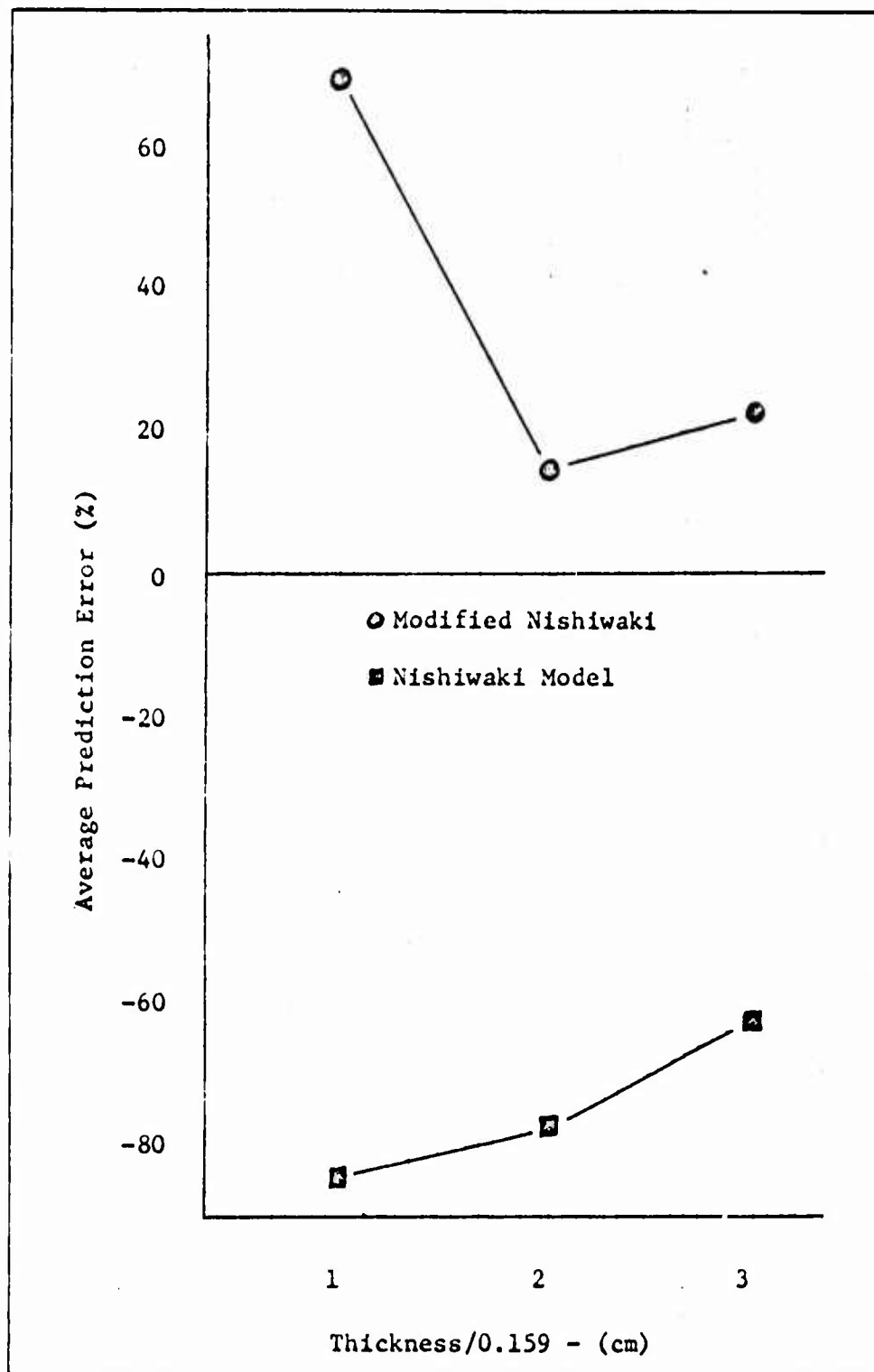


Fig. 14. Comparison of Velocity Loss  
Prediction Error for Optimal Projectiles

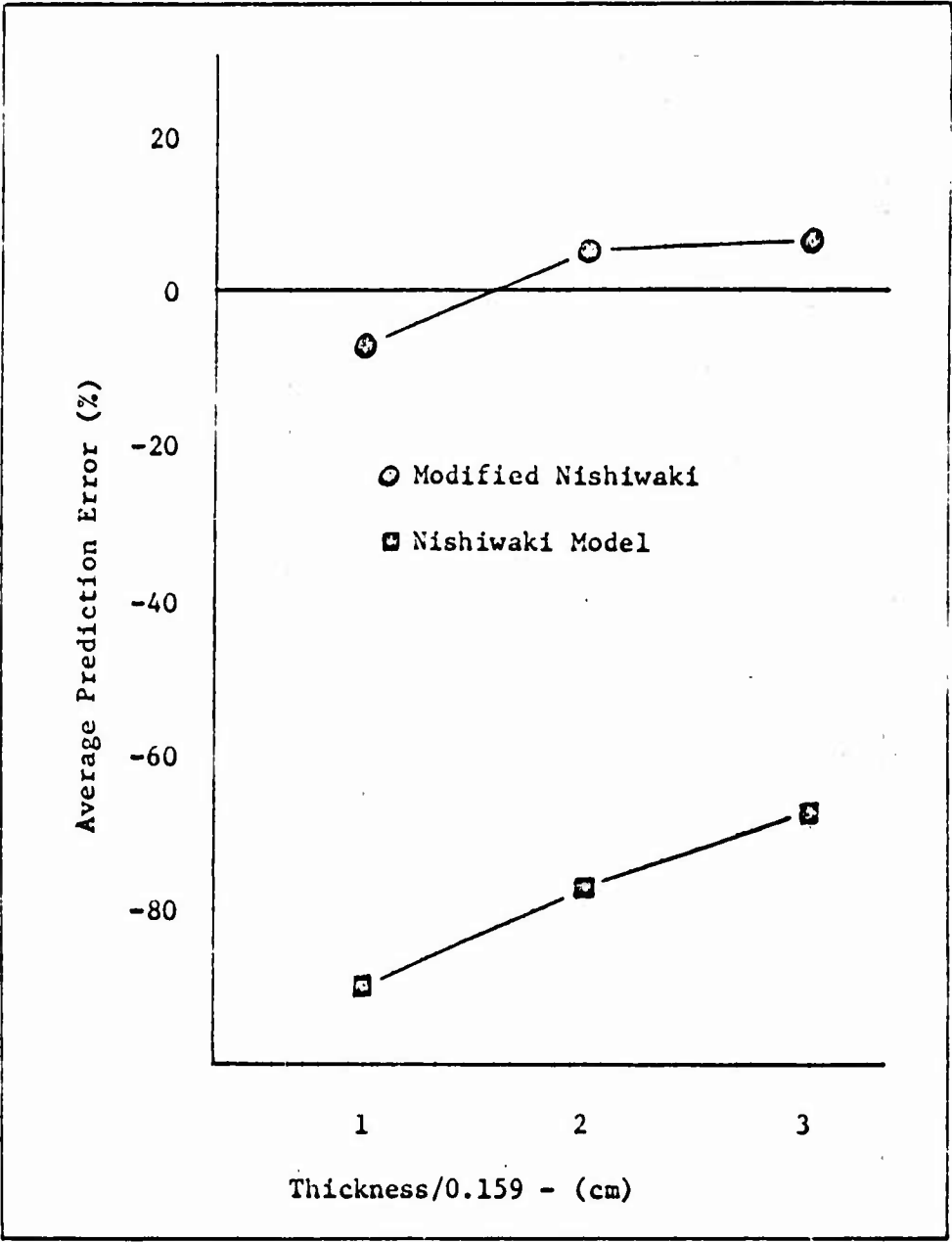


Fig. 15. Comparison of Velocity Loss Prediction Error for Russian Projectiles

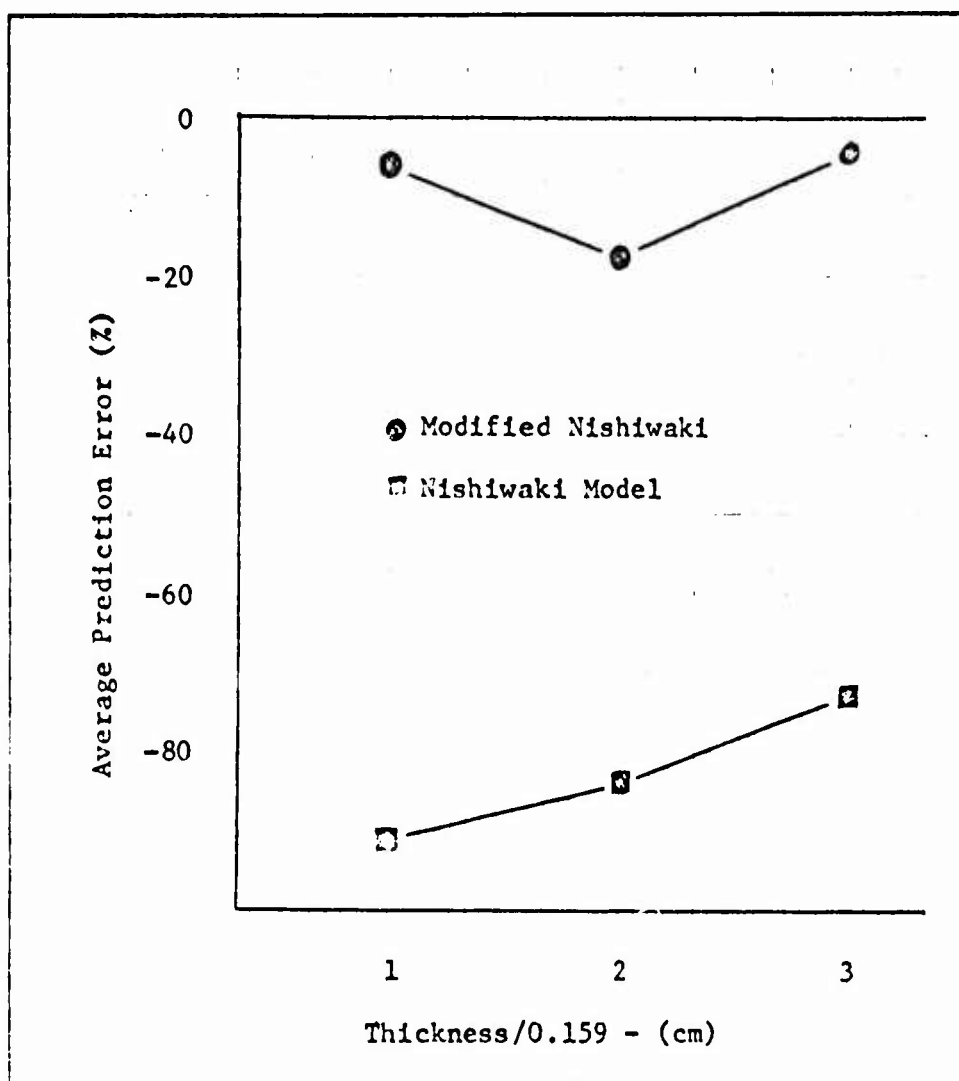


Fig. 16. Comparison of Velocity Loss Prediction Error for Ball Projectiles

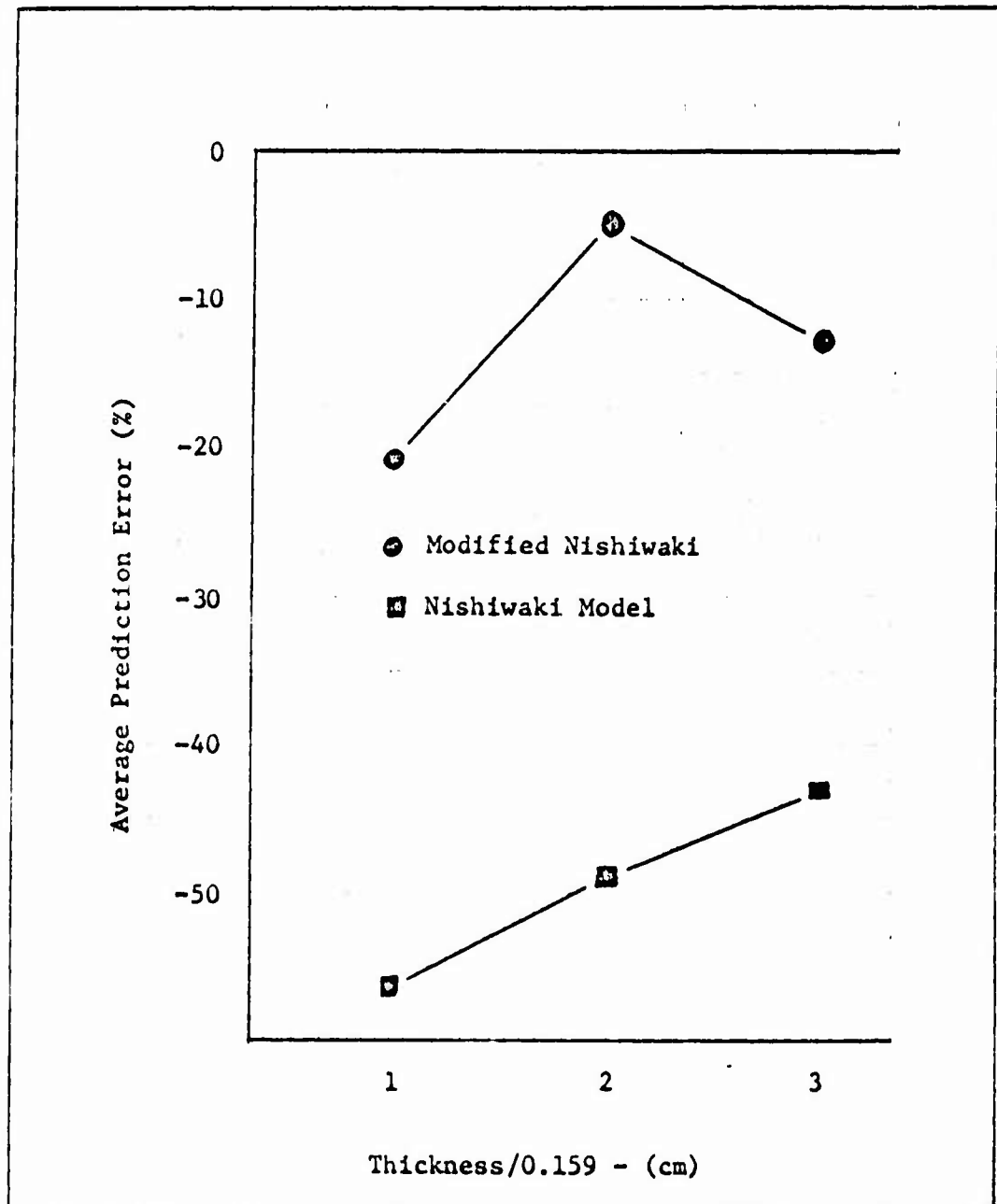


Fig. 17. Comparison of Velocity Loss Prediction Error for Cone #1 Projectiles

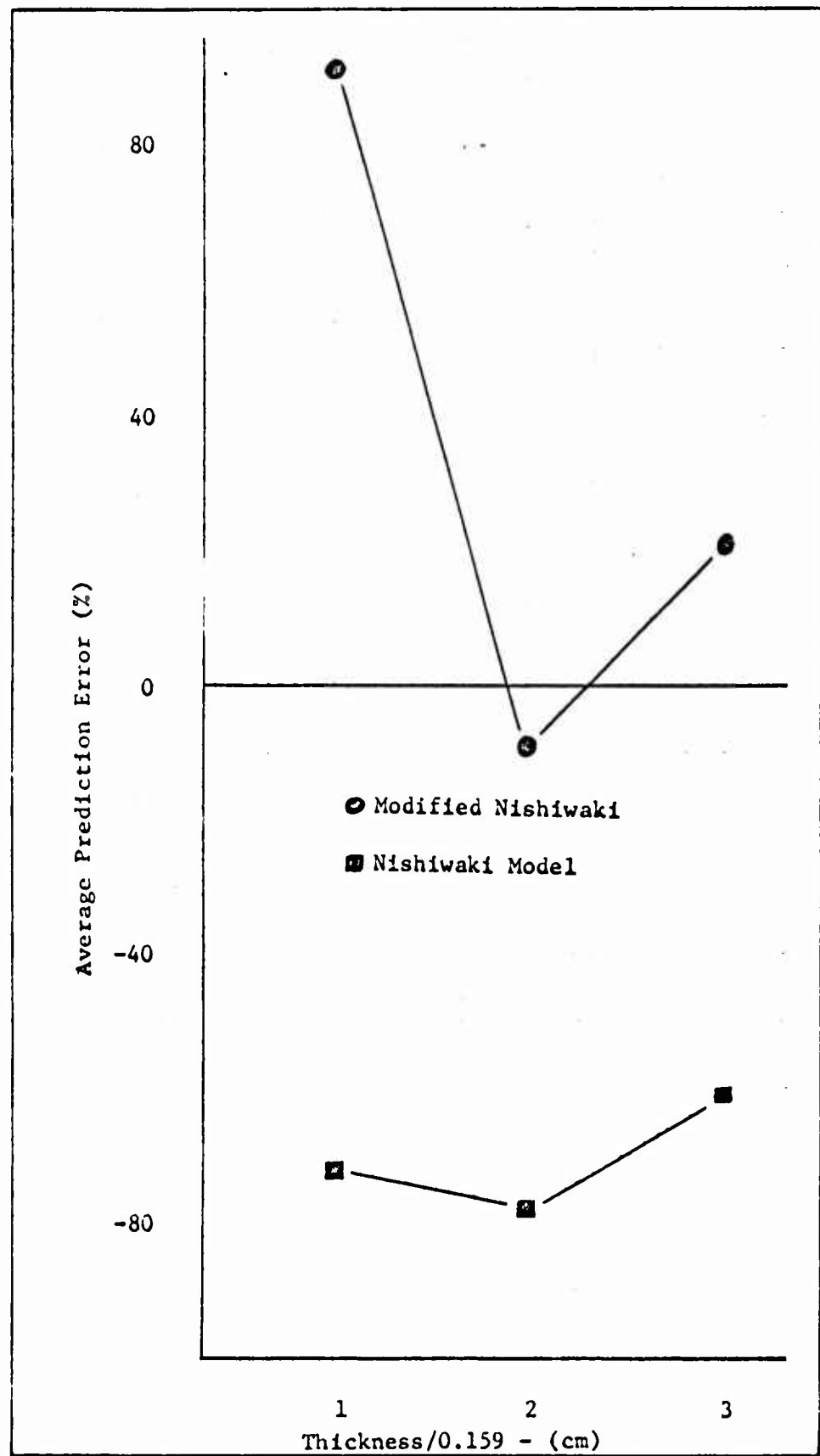


Fig. 18. Comparison of Velocity Loss Prediction Error for Cone #2 Projectiles

predicted velocity loss and probably decrease the error. Projectiles such as the ball and cylinder reflect the least prediction error. This corresponds to the fact that these two shapes eject plugs almost equal in diameter to the projectile. In addition, the magnitude of the error for these two shapes is almost at the limit of experimental accuracy.

Ballistic limit predictions for meter cylindrical projectile of varying mass against targets of 0.159, 0.317, and 0.476 cm 6061-T6 aluminum targets are shown in Fig. 19.



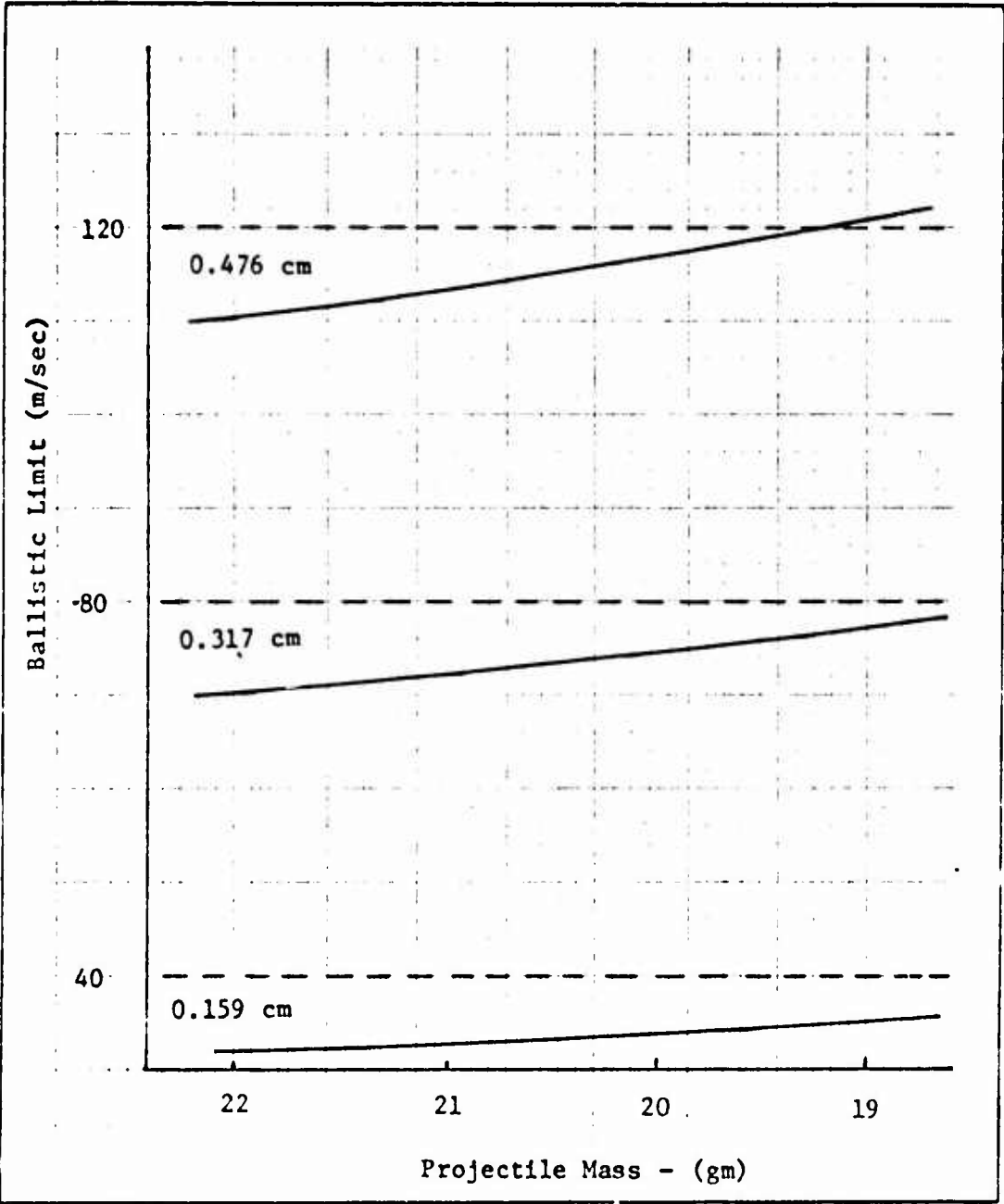


Fig. 19. Predicted Ballistic Limit of 6061-T6 Aluminum Impacted by Cylindrical Projectiles

## V. Conclusions and Recommendations

### Conclusions for Static Experiments

The experimental technique used in this study to determine the Nishiwaki static pressure coefficient ( $P_0$ ) appears to result in a reasonably accurate approximation for this term. Although there is some evidence to the contrary, it seems reasonable to assume that  $P_0$  is universal for a given target thickness and constant for a low impact velocity range. The increase in impact velocity required to result in a significant change in  $P_0$  appears to be considerable. In addition, the technique used in this study produced values of  $P_0$  quite similar to those obtained by Nishiwaki while taking much less time.

The force versus time reactions for various projectiles appear to be consistent for all penetration rates and target thicknesses used in this study. These curves are similar in behavior to those that would be obtained if the Nishiwaki static pressure coefficient term were plotted as a function of penetration depth.

It appears possible to ascertain the geometry of a plug any projectile would eject on dynamic impact, implying the mass and shape of the plug might be predictable as a function of projectile geometry and target properties.

Theoretical force versus time curves could possibly be used to predict the projectile velocity loss due to the static reaction of the target, leaving only a calculation of the energy imparted to the plug to accurately predict residual velocity and projectile penetration efficiency.

### Conclusions for Dynamic Experiments

The Nishiwaki equations proved to be quite accurate for cylinders when the experimental value of  $P_0$  was used. However, results for other shapes showed relatively high error. In addition, the order of magnitude of the integrating factor for curved shapes (Appendix D) virtually eliminates dynamic considerations of ejected plugs.

The Modified Nishiwaki Theory, which assumes creation of a plug equal in diameter to the projectile for all shapes, resulted in fairly accurate residual velocity predictions. A proper correction for the size of the ejected plug could improve the accuracy of this approach.

With regard to experimental technique, sufficient accuracy in impact and residual velocities can be obtained using the system outlined in this study. It is possible to obtain projectile behavior approaching the ideal as to impact orientation, no projectile deformation, and suitable stability after impact.

### Overall Conclusions

The basic analysis by Nishiwaki, with the appropriate modifications, appears to lead to a plausible theory of penetration. While the original Nishiwaki equations, which assume virtually no plugs, tend to predict less of a velocity drop than actually occurs, the Modified Nishiwaki tends to predict more of a velocity drop than is observed experimentally. The magnitude of error appears to correlate with the size of the actual plug ejected by the specific projectile shapes. Although the magnitude of error in both analyses is still too large, the apparent trend of the data seems to be approaching increased accuracy.

Recommendations

The following recommendations are based on the results and experimental methods of this study.

- a. More static tests should be performed to attempt to determine plug geometry and mass as a function of projectile shape and target thickness.
- b. These static tests should be extended to thicker targets of 6061-T6 aluminum and expanded to include other types of aluminum.
- c. Additional dynamic tests should be performed, using the techniques described in this study. To improve the significance of the data and amplify dynamic effects, much lower impact velocities and some thicker targets should be used to increase the magnitude of the projectile velocity loss.
- d. Further low temperature static testing should be performed to determine the behavior of the static pressure coefficient ( $P_o$ ) as a function of impact velocity.
- e. Additional analysis of the force versus time data obtained in static experiments could be made to see if penetration efficiency might be determined in this manner.
- f. Other forms of the Nishiwaki approach, as stated earlier in this study, could be evaluated when additional data is available.

Bibliography

1. Bertke, R.S. "The Air Force Materials Laboratory Terminal Ballistic Research Facility," Technical Report AFML-TR- 69-215, October 1969, Air Force Materials Laboratory, Wright-Patterson Air Force Base, Ohio.
2. Bethe, H.A. "Attempt of a Theory of Armor Penetration" for Frankford Arsenal, 1941.
3. Butcher, B.M. and C.H. Karnes. "Strain-Rate Effects in Metals." J. of Appl. Physics, 37:1, 402-411 (January 1966).
4. Catalog of Foreign Material, Vol. 1 (Combat Material). FSTC 381-3004 (Secret), January 1963, U.S. Army Foreign Science and Technology Center, Washington, D.C.
5. Craggs, J.W. "The Normal Penetration of a Thin Elastic-Plastic Plate by a Right Circular Cone," University College, Dundee, October 1952.
6. Fields, T.E. "The Effect of Projectile Shape on the Ballistic Perforation of Thin Metal Plates." Technical Report AFML-TR-69-202, July 1969, Air Force Materials Laboratory, Wright-Patterson Air Force Base, Ohio.
7. Freiburger, W. "A Problem in Dynamic Plasticity: The Enlargement of a Circular Hole in a Flat Sheet," Proc. of Cambridge Phil. Soc., 48:135-148 (1952).
8. Giere, A.C. "Some Energy and Momentum Considerations in the Perforation of Thin Plates." AIAA Journal, 2:8, 1471-1472 (August 1964).
9. Goldsmith, Werner. Impact, London: Edward Arnold (Publishers) Ltd., 1960.
10. Krafft, Joseph M. "Surface Friction in Ballistic Penetration." J. of Appl. Physics, 26:10, 1248-1253 (October 1955).
11. Kucher, V.B. "Optimum Projectile Design for Armor Penetration." Maryland: Ballistic Research Laboratories Rpt. No. 1379 (November 1967).
12. Nishiwaki, Jien, "Resistance to the Penetration of a Bullet Through an Aluminum Plate." J. Phy. Soc. of Japan, 6:374-378 (October 1951).
13. Rinehart, John S. and John Pearson. Behavior of Metals Under Impulsive Loads, New York: Dover Publications, Inc., 1960.
14. Stronge, William J. "Comments on 'Some Energy and Momentum Considerations in the Perforation of Thin Plates'." AIAA Journal,

3:3, 570-571 (March 1965).

15. Taylor, G.I. "The Formation and Enlargement of a Circular Hole in a Thin Plastic Sheet." J. of Mech. and Appl. Math., 1:103-124 (March 1948).
16. Thomson, William T. "An Approximate Theory of Armor Penetration." J. of Appl. Physics, 26:1, 80-82 (January 1955).
17. Zaid, Melvin and Paul Burton. "Mechanics of High Speed Projectile Penetration." J. of Franklin Inst., 264:117-126 (1957).

## Appendix A

Description of Equipment

The Air Force Materials Laboratory Low Velocity Impact Test Range was used for dynamic testing in this study. This laboratory is located in Building 44, Area B, Wright-Patterson Air Force Base, Ohio. The range is operated by the University of Dayton Research Institute under Air Force contract. The range equipment consisted of the gun, sabot catch tank, velocity measurement systems, photographic system, and flash X-ray systems. A diagram of range geometry is shown in Fig. 20.

The Metallurgy and Ceramics Research Laboratory was used for static testing in this study. This laboratory is a division of the Air Force Aerospace Research Laboratories, located in Building 450, Area B, Wright-Patterson Air Force Base, Ohio. The Instron Model TT was used in the static tests and a diagram of the apparatus is given in Fig. 21.

Gun (Ref 1:7)

The gun is a Frankford Mann universal mount with a 50 caliber barrel, rifled for one revolution per 25.4 cm of travel. The projectiles and sabots were loaded in 50 caliber cartridges and percussion fired by a remote control electric solenoid.

Sabot Catch Tank (Ref 1:15)

The copper sabots were trapped in a steel sabot catch tank located 50 cm in front of the gun barrel. The projectile and sabot entrance hole is 38 cm in diameter while the projectile exit hole is 8 cm in

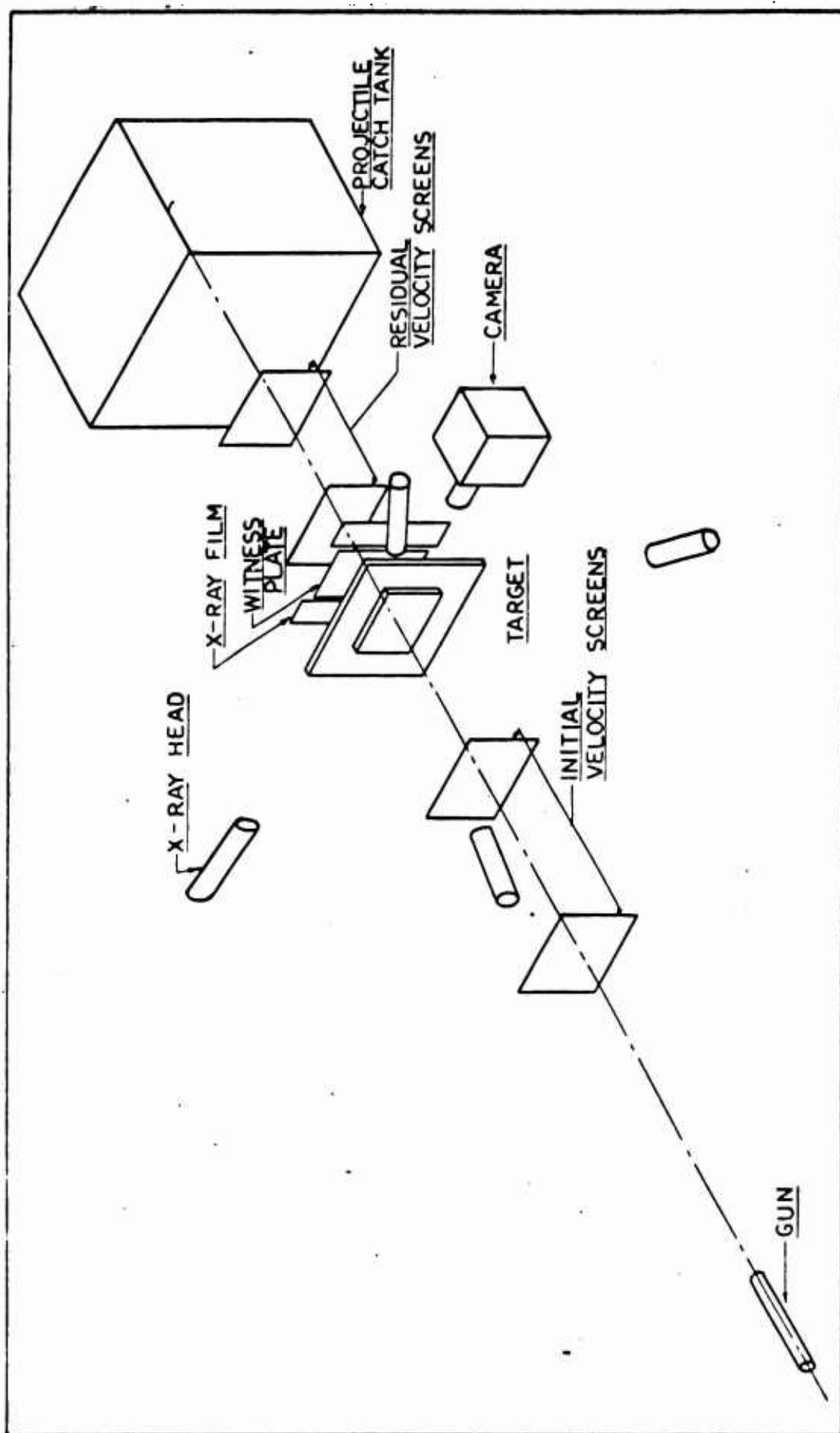


Fig. 20. Range Layout



diameter. The sabots were stopped by seven layers of plywood.

Contact Switches (Ref 1:19)

Aluminum foil and mylar were sandwiched to provide switches to trigger the velocity chronographs, photographic witness plate, and X-ray equipment. A potential of 600 volts was applied across the switches, triggering an electrical pulse when the switch was perforated by the projectile.

Chronographs (Ref 1:19)

Initial projectile velocity was determined by measuring the time required to transverse the distance (1.2 m) between two contact switches located 1.8 m and 3.0 m in front of the target. This time was recorded to the nearest microsecond by a Beckman Universal EPUT and Timer, Model 7360A. Initial velocities were calculated within 0.05m/sec. A Beckman/Berkly Universal EPUT and Timer recorded, to the nearest microsecond, the time elapsed between X-ray photographs. Residual velocities were calculated from the time recorded and the displacement of the projectile recorded on the two X-rays.

Flash X-ray System (Ref 1:21)

Projectile residual velocities, orientation, and stability were determined from X-rays taken when the projectile was approximately 30 cm and 100 cm past the point of target impact. Two 150 kv vlash X-rays were used. The system included two X-ray heads located along and 120 cm above the trajectory, two film cassettes located directly below the heads 26 cm below the trajectory, and a Field Emission Corporation Model 154 four channel control unit. The X-rays were

triggered directly from the contact switches.

Static Test Equipment

The prototype Instron Model TT was used in quasi-static penetration tests. It is capable of recording a maximum applied load of 50,000 pounds in either tension or compression. It provides constant penetration rates from 8.5 mm/sec down to 0.0002 mm/sec. A diagram of this equipment is given in Fig. 21.

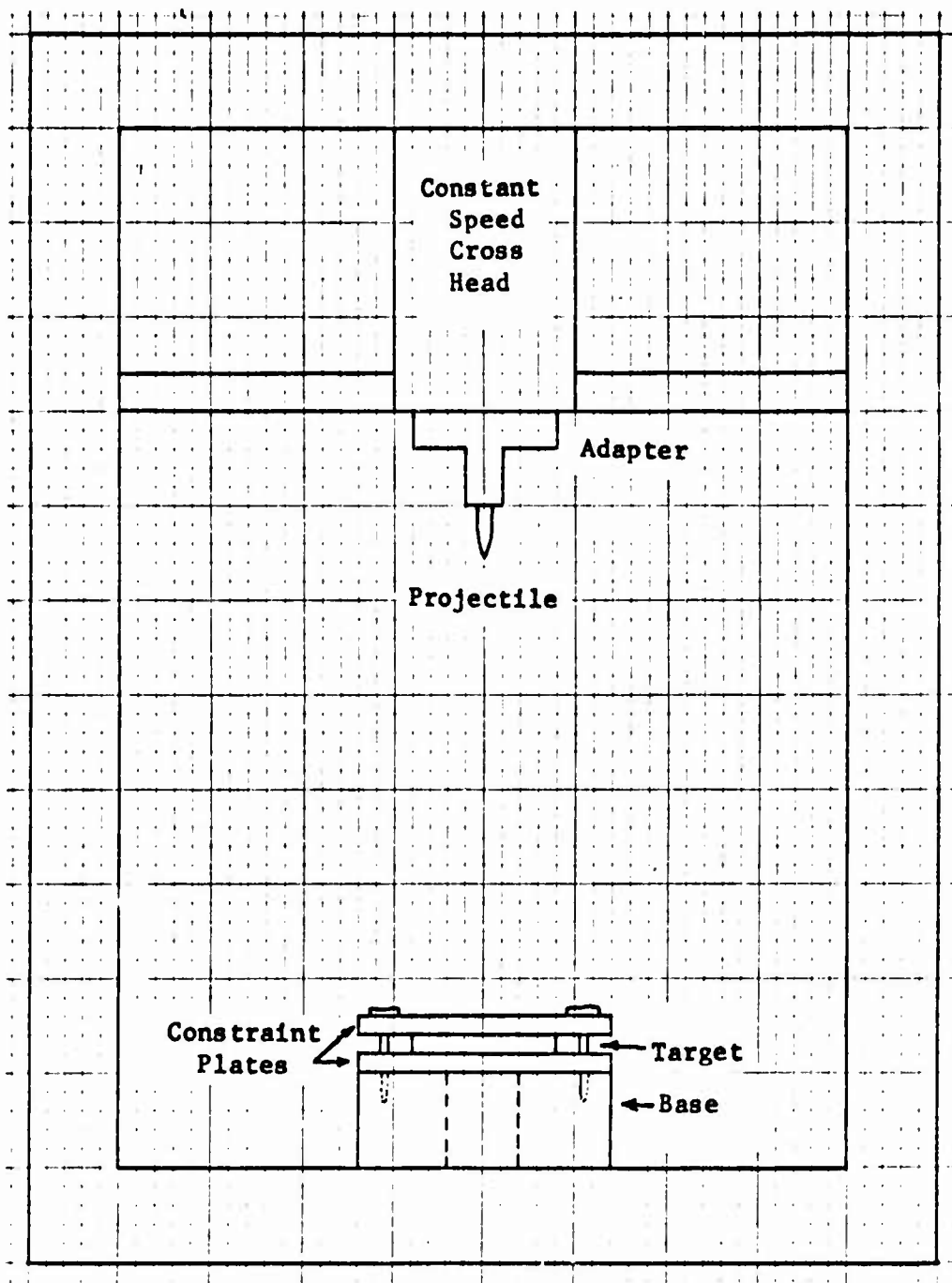


Fig. 21. Schematic of Instron Model TT

## Appendix B

Projectile Design

The Ogive, Russian, Optimal, Cylinder, and Cone #1 shaped projectiles used in this study were left over from the experiments conducted by Fields (Ref 6). The Cone #2 and Ball design were manufactured for this study. All projectiles were made of 1.11 cm diameter tempered steel drill rod. Each projectile was notched to provide a method to crimp the sabots to the projectiles. The relative shape of the projectiles is given in Fig. 23.

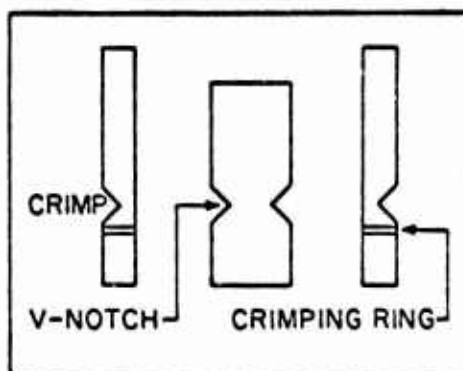


Fig. 22. Sample Projectile and Sabot (From Ref 6:53)

Projectile Sabots

The sabots were manufactured from half-hard copper tubing 0.89 mm thick, 1.27 cm in diameter and 3.49 cm in length. The tubing was split lengthwise to form the two sabot halves. A 0.127 mm deep groove, 0.8 mm wide, was cut in the outer surface of the sabot a distance of 6.4 mm from the base. The cartridge was crimped into this groove during loading. A diagram of a sample projectile and sabot is shown in Fig. 22.

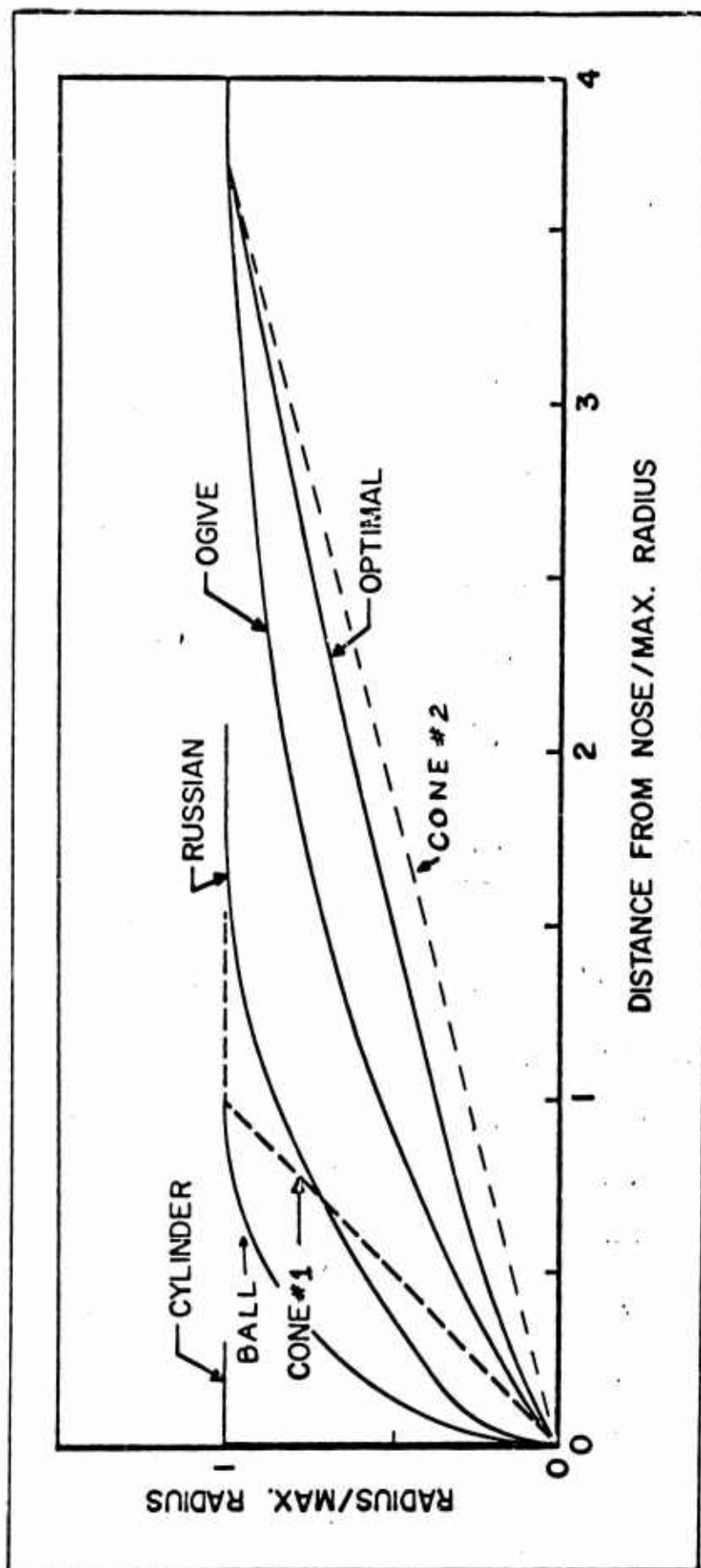


Fig. 23. Comparison of Projectile Nose Shapes

Ogive Shape

This shape was patterned after the core of a U.S. 50 caliber armor piercing bullet. The Ogive projectiles were  $3.49 \pm 0.01$  cm long with an average mass of 19.31 gm (Ref 6).

Russian Shape

The Russian shape was designed from the core of a 14.5 mm Russian armor piercing bullet. Its length was  $3.17 \pm 0.01$  cm with an average mass of 19.66 gm (Ref 6).

Optimal Shape

This projectile was designed from Kucher's equation (Ref 15:11) for an optimal penetrator of thin plates. The total length was  $3.49 \pm 0.01$  cm with an average mass 19.38 gm (Ref 6).

Cone #1

This Cone was  $3.17 \pm 0.01$  cm in length with an average mass of 19.7 gm. The nose cone had a semi-vertex angle of 45 degrees (Ref 6).

Cone #2

This Cone was  $4.23 \pm 0.01$  cm in length with an average mass of 20.82 gm. The nose cone had a semi-vertex angle of 15.1 degrees.

Cylinder

The cylindrical shape was  $2.86 \pm 0.01$  cm in length with an average mass of 19.88 gm (Ref 6).

Ball

The Ball shape was a hemispherical nose shape of radius 0.555 cm. The overall projectile was  $3.04 \pm 0.01$  cm in length with an average

GAW/MC/70-2

mass of 20.65 gm.

## Appendix C

Data and Data Reduction

In this investigation, data was obtained from three basic measurement techniques; a chronograph for initial velocity, timed X-ray photographs for projectile residual velocity, and the Instron Model TT for static pressure loads.

Initial Velocity Data

The initial projectile velocity was calculated from measurements of the time required to travel a measured distance between contact switches. A chronograph recorded the time to the nearest microsecond and the velocity determined to the nearest 0.05 m/sec with a maximum error of  $\pm 0.25\%$ .

Impact Velocity Data

A projectile of each shape (Ball and Cone #2) was fired downrange with no target. Initial and residual velocities for aerodynamic drag were calculated. A drag force proportional to the square of the velocity was assumed. The equation of motion used was:

$$DV^2 = m \frac{dV}{dt} \quad (10)$$

where  $m$  is the projectile mass,  $V$  is the projectile velocity, and  $D$  is the drag coefficient. A computer program was used to determine the drag coefficient and impact velocities directly.

X-ray Measurements

The basic purpose of the flash X-ray measurements was to determine projectile residual velocities and orientation, and as a method



of observing any plugs.

Relative positions between the two X-rays were measured with a scale prepared from X-ray photographs of a reference positioned along the trajectory. Wire cross hairs on each film holder and drill holes in the reference provided a measurement of the distance traversed by the projectile between the two X-ray photographs. The time between X-rays was measured to the nearest microsecond by chronographs. Projectile residual velocities were calculated from these measurements.

#### Static Pressure Measurements

The Instron Model TT was used to measure, to three significant figures, the total load along the axis of a projectile during static penetration. Both the rate of penetration and chart speeds were constant during the tests. The resultant charts, therefore, display both force versus time and force versus depth of penetration. The plot of force versus time for the cylinder was used to determine the static pressure coefficient ( $P_0$ ), since curves for all other shapes included a component of surface friction not taken into account in dynamic impact. The average peak value of the force curve at all three penetration rates was used as the load and the cross sectional area of the cylinder used as the area to determine  $P_0$  for each thickness. The experimental values of  $P_0$  were not linearly proportional to the target thickness, as claimed by Nishiwaki, so actual values were used in all computations. The value of  $P_0$  for 6061-T6 aluminum was found to be:

(7.17)  $\text{kg/mm}^2$  for 0.159 cm targets

(17.8)  $\text{kg/mm}^2$  for 0.317 cm targets

(28.7) kg/mm<sup>2</sup> for 0.476 cm targets

The area of deformation was confined by plates on either side of the target material to maintain a deformation area equal to that observed in dynamic tests. Any difference in target appearance after penetration by dynamic and quasi-static methods was not detected by visual observation. It is felt, therefore, that the static penetration tests closely approximated the dynamic behavior of perforation. Sample typical force versus time plots for all shapes against a given thickness are shown in Figs. 10 and 11. Typical plots showing the variation of force versus time for various thicknesses are shown in Fig. 9. The consistency of the data for a given shape and thickness for different penetration rates is shown in Fig. 8.

## Appendix D

Solution of Nishiwaki EquationsSolution of Nishiwaki Equation for Curved Shapes

For hemispheric nose shape projectiles, the Nishiwaki equation reduces to:

$$M \frac{dV}{dt} = -2 P_o \int (r-x) dx - \frac{V^2 2\pi\rho}{r^2} \int (r-x)^3 dx \quad (11)$$

which can be written:

$$\frac{dV}{dt} = -K_1 f(x) - V^2 K_2 g(x) \quad (12)$$

The general development of the equation, within the appropriate limits, is as follows:

$$VdV = -K_1 f(x) dx - V^2 K_2 g(x) dx \quad (13)$$

$$2VdV + V^2 2K_2 g(x) dx = -2K_1 f(x) dx \quad (14)$$

$$d \left( V^2 e^{\int 2K_2 g(x) dx} \right) = -2K_1 \int f(x) e^{\int 2K_2 g(x) dx} dx \quad (15)$$

The value of the integrating factor,  $e^{\int 2K_2 g(x) dx}$  was evaluated for all values of  $x$  over the limits and was found to vary between 0.9865 and 1.000 in value. This accounts for the large errors in predicting residual velocity for severely curved shapes since the dynamic term

is virtually eliminated. This implies there would be no plug, or a small one at best, for the Ball shape projectile. However, X-ray photographs of the Ball projectile immediately after impact show a plug leading the projectile. The diameter of the plug closely approximated the diameter of the projectile, implying dynamic effects similar to that of the Cylinder shape. For other projectiles with a curved nose shape, similar differential equations result. Residual velocity calculations for all curved shape projectiles included approximation techniques on the integrating factor.

#### Solution of Alternate Analysis of Nishiwaki Model

For the free body diagram included in Fig. 4, the equations of motion for the projectile, static target material, and impacted target material may be written.

For a projectile of mass  $M$ , velocity  $V$ , and a net interface with the target of area  $A$ , the equation of motion is:

$$M \frac{dV}{dt} = - \int_A F_1 dA_1 \sin \alpha \quad (16)$$

Since the sum of forces acting on the static target material is zero, the equation of motion of the target may be written:

$$\int_A F_1 dA_1 \sin \alpha - P - \int_A G_1 dA_1 \sin \alpha = 0 \quad (17)$$

The displaced particles of target material are assumed to move normal to the projectile surface with a velocity equal to  $V \sin \alpha$ , the equation of motion for these particles may be expressed:

$$\sum_A \rho V^2 \sin^3 \alpha \, dA_1 = \sum_A G_1 \, dA_1 \sin \alpha \quad (18)$$

Summing the three equations, the net equation of motion for the system may be written:

$$M \frac{dV}{dt} = - \sum_A \rho V^2 \sin^3 \alpha \, dA_1 \quad (19)$$

If one assumes that the resultant force  $P$  is composed of the summation of forces per unit area normal to the projectile surface acting on the area of interface, then the force  $P$  may be expressed as:

$$P = \sum_A P_1 \sin \alpha \, dA_1 \quad (20)$$

This results in an equation similar to that derived by Nishiwaki:

$$M \frac{dV}{dt} = - \sum_A (P_1 + \rho V^2 \sin^2 \alpha) \sin \alpha \, dA_1 \quad (21)$$

Vita

Richard David Gabbert was born on 31 December 1936 in Chicago, Illinois. He graduated from high school in 1954 and attended Illinois Institute of Technology prior to enlisting in the Air Force in 1955. After training in the Chinese Language at Yale University, he served as a linguist in Japan and Korea with an intelligence organization. After returning to the United States, he was selected for the Airmen Education and Commissioning Program and assigned to the University of Oklahoma. He received the degree of Bachelor of Science in Aeronautical and Space Engineering in 1964 and was elected to Tau Beta Pi and Sigma Gamma Tau. Upon completion of Officer Training School, he was assigned to the Aircraft Maintenance Officer Training School at Chanute Air Force Base, Illinois. Prior to his selection for graduate school, he served as an aircraft maintenance officer with the Tactical Air Command at Eglin Air Force Base, Florida.

Permanent Address: 6851 Stonehurst Drive  
Dayton, Ohio - 45424

This thesis was typed by Mrs. Katherine Randall